Chapter 4
Methodology of SSM Characterization

Abstract The microstructure of the SSM alloy billets plays an important role during fabrication of finished engineering component and its performance in service. As a result, it is critically important to characterize the microstructure to ensure high-quality feed stock. This chapter provides a detailed account of the characterization techniques available to SSM researcher to confidently examine the quality of as-cast billets through thermal analysis, rheological characterization, and quantitative metallography.

Conventional solidification of hypoeutectic Al–Si foundry alloys takes place with dendritic formation of primary α-Al phase within the liquid. The alloy composition, temperature gradient within the melt, thermo-fluid convection, and rate of heat extraction and the resulting constitutional supercooling are the most effective parameters on the morphology of the primary α-Al phase. Variation of any of these factors during solidification would alter the as-cast structure. For instance, introduction of agitation (forced convection) into the solidifying melt changes the distribution of alloying elements and localized chemical composition, could remove constitutional supercooling, and promote dendrite-to-equiaxed transition, i.e., break down and globularization of the α-Al phase. Degeneration of the α-Al phase results in some opportunities which are of interest from commercial viewpoints.

The advantages of the SSM processing along with different available technologies as discussed in Chap. 2 are enormous. However, the lack of industrial interest in the 80s and 90s stemmed mainly from the high cost of billet preparation, the issue of recycling the returned and scraped parts, and to some extent the lack of proper characterization of the both semifinished billets and finished engineering components. Recently, the cost issue is resolved by introducing novel cost-effective rheocasting techniques and development of new alloying systems.

In order to generate a semi-solid structure, the alloy system plays the key role where the coexistence of liquid and solid within a temperature range is the prerequisite for the slurry preparation. The mechanics and mechanisms of the primary particles' evolution, dendrite to equiaxed transformation, is the next concern since the formation of globular morphology is expected to enhance die filling and improve mechanical properties of as-cast parts. The ideal microstructure for SSM slurry is fine spherical solid particles uniformly distributed within a liquid matrix.

S. Nafisi, R. Ghomashchi, *Semi-Solid Processing of Aluminum Alloys*,
DOI 10.1007/978-3-319-40335-9_4

The solid fraction should be considered carefully, since low fraction solid may lead to SSM slurry handling and mold filling difficulties due to insufficient viscosity and turbulence while high fraction solid adversely affects the die filling and requires more powerful machinery and thus increase the cost of manufacturing.

Based on the aforesaid requirements, characterization of semi-solid material is a necessity to confirm, modify, and obtain optimum structure for SSM-shaped components. This knowledge not only provides an idea about the material, but also leads to better understanding of rheological behavior and eventually improve the mechanical properties of cast pieces.

The term "*characterization*" covers a wide range of thermal, mechanical, and microstructural analytical techniques used to evaluate physical, mechanical, and metallurgical parameters of SSM billets and finished products. The SSM billets are often required to be examined for their solidification pattern, rheological behavior, and microstructure. The outcome of such studies helps in understanding / predicting the fluid flow and die-filling behavior of the SSM billets along with the possible mechanical and load-bearing characteristics of finished product.

The following sections provide an account of thermal (solidification), rheological, and structural methods available to characterize SSM products. In addition, the experimental procedures employed to prepare samples for characterization of SSM billets are also explained.

4.1 Solidification Characterization

The quality of finished product is tied up with the quality of feedstock (billets). The integrity of the billets, however, is dependent on the SSM processing parameters and these parameters are interpreted in terms of solidification condition. The cooling curve is the fingerprint of an alloy solidification behavior as it provides information on nucleation and growth of phases form during liquid to solid transformation. The following explains how the solidification behavior of the billets should be monitored and characterized.

Following the preparation of molten alloy in a resistance heating furnace, melting of Al–Si ingots and degassing using argon, a portion of the molten charge was poured into graphite cups of 25 mm inner diameter and 5 mm wall thickness (Fig. 4.1). Cups were held inside the crucible for approximately 1 min prior to tests to reach equilibrium condition ensuring uniform temperature distribution across the sample at the beginning of solidification. Each cup with ~50 g of alloy was transferred to the testing platform and two K-type thermocouples (0.8 mm diameter) were quickly immersed into the melt near the center and wall of the mold with their tips at 10 mm from the mold bottom. Temperature readings were collected by a high-speed high-resolution data acquisition system (National Instrument SCXI-1102) at ten readings per second sampling rate. To ensure the radial heat flow, insulating plates were placed above and below the sample cup. To improve data consistency and reproducibility, the same thermocouples were used for all tests by

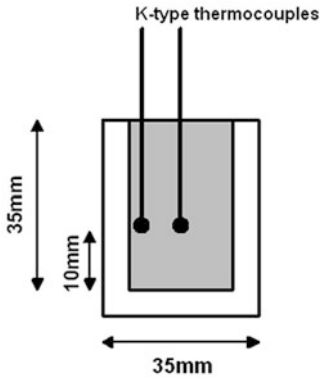

Fig. 4.1 Graphite cup geometry for thermal analysis purpose

placing the thermocouples in a 1 mm (inner diameter) stainless steel sheath. The protective sheath saved thermocouples after solidification where they could be easily removed from sample and reused.

As for metallography, transverse section at the tip of the thermocouples was cut and for consistency of results, the area between the center and the wall of the entire samples was examined (quarter area).

According to the literature, the cooling rate can either be calculated above liquidus temperature or in the mushy zone. However, the cooling rate is often registered high right after mold filling due to initial rapid heat dissipation. The cooling rate gradually slows down in the mushy zone. As an example, the cooling rates for the graphite molds used were between 1.5–2 $^{\circ}Cs^{-1}$ and 0.5–0.6 $^{\circ}Cs^{-1}$ above the liquidus and in the mushy zone, respectively. The analysis of the thermal data was carried out following Backerud et al. and Tuttle [1, 2]. Since there are some dissimilarities in the definition of the critical parameters in the literature, the following nomenclatures are defined in this book. The points are also identified on an actual cooling curve in Fig. 4.2 (only for graphite cup samples):

- $T_{\mathrm{nuc_{Al}}}$: Start of primary α-Al dendrites nucleation
- $T_{\mathrm{min_{Al}}}$: Unsteady state growth temperature, the temperature beyond which the newly nucleated crystals grow to such extent that the latent heat liberated surpasses the heat extracted from the sample
- $T_{\mathrm{g_{Al}}}$: Recalescence of steady-state growth temperature due to release of latent heat of primary α-Al dendrites
- ΔT_{Rec}: Temperature difference between unsteady ($T_{\mathrm{min_{Al}}}$) and steady ($T_{\mathrm{g_{Al}}}$) state growth temperatures of primary α-Al particles (recalescence)
- t_{Rec}: Recalescence time, time difference between $T_{\mathrm{min_{Al}}}$ and $T_{\mathrm{g_{Al}}}$, the times associated with $T_{\mathrm{min_{Al}}}$ and $T_{\mathrm{g_{Al}}}$ (in the literature, it was labeled as liquidus undercooling time [2, 3])
- $T_{\mathrm{nuc_{eut}}}$: Start of eutectic nucleation
- $T_{\mathrm{min_{eut}}}$ and $T_{\mathrm{max_{eut}}}$: Minimum and maximum of eutectic temperatures
- $\Delta\theta$: Variation of eutectic recalescence ($T_{\mathrm{max_{eut}}} - T_{\mathrm{min_{eut}}}$)

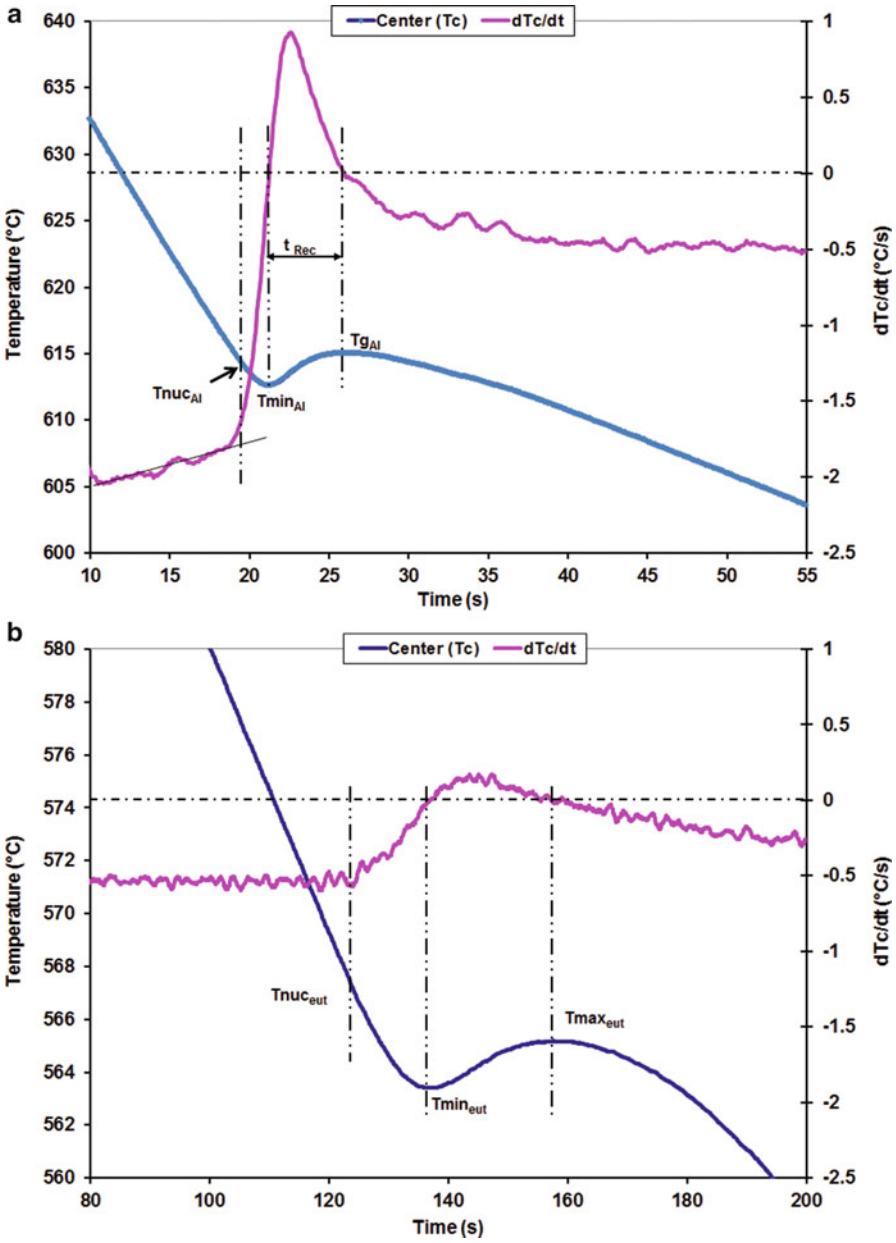

Fig. 4.2 Cooling curve and first derivative of 356 alloy: (**a**) α-Al formation region, (**b**) eutectic region

- T_{end}: Solidification termination
- ΔT_{α}: α-Al solidification range ($T_{nuc_{Al}} - T_{nuc_{eut}}$)
- ΔT_{eut}: Eutectic solidification range ($T_{nuc_{eut}} - T_{end}$)

Undercooling was defined in many academic literatures (e.g., [4]) as the difference between $T_{min_{Al}}$ and $T_{g_{Al}}$ with $T_{min_{Al}}$ defined as the starting point of solidification. The authors would like to reemphasize on the finding of Backerud et al. [1] where the actual solidification starts above the $T_{min_{Al}}$ and it is detectable by the first derivative ($\frac{\partial T}{\partial t}$) curve as shown in Fig. 4.2. The change in the slope of $\frac{\partial T}{\partial t}$ is an indication of energy change in the system and the only energy change during solidification is the formation of solid phase, start of nucleation. So if the solidification start is the point shown in Fig. 4.2, then how undercooling can be defined as undercooling is an integral requirement to trigger nucleation and to onset solidification. The actual undercooling may be defined as the difference between the equilibrium melting temperature (discernable from equilibrium phase diagram) and the $T_{nuc_{Al}}$. Therefore, the value of ($T_{min_{Al}} - T_{g_{Al}}$) is neither undercooling nor nucleation range and can only be defined as the recalescence range (of note that this topic is not intended to be opened in this book).

Chemical composition of the melt plays an important role in the thermal analysis results. As for instance, the liquidus temperature of the Al–Si melts varies with Si% according to the following equation (4.1) [5]:

$$T_l(^{\circ}\mathrm{C}) = 662.2 - 6.913 * [\%\mathrm{Si}] \tag{4.1}$$

So, by a simple calculation, it is evident that a compositional difference of 0.1% Si between two samples means a difference of about 0.7 °C. Hence the chemistry variation is a key in the cooling curve analysis.

4.1.1 Various SSM Processing

The solidification characterization is explored in the context of four SSM processing routes as detailed below.

4.1.1.1 Rheocasting, Low Pouring Temperature Technique

As indicated in Chap. 2, among different techniques available for SSM processing, casting at low superheat is regarded as the least expensive alternative to produce thixo/rheo billets. For these series of tests, the molten metal was poured into a coated cylindrical steel mold of 75 mm diameter and 250 mm long and the bottom of the mold was sealed by a refractory material. After melt preparation, the alloy was poured at different superheats, in the range of ~ 0–80 °C. Prior to pouring, the mold was tilted to reduce the turbulence. Figure 4.3 shows schematically the actual

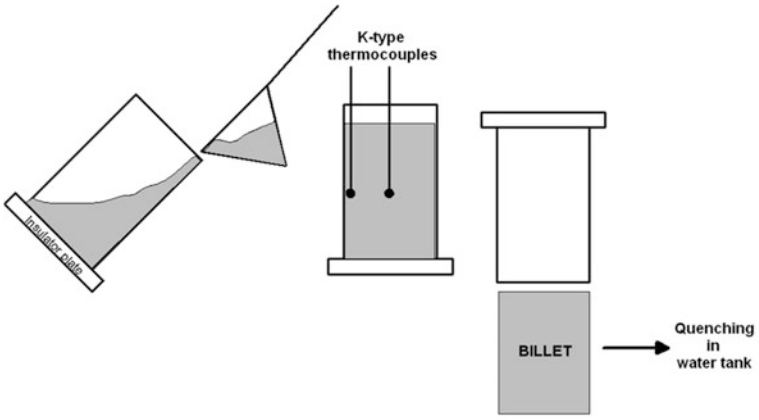

Fig. 4.3 Schematic of low pouring temperature process

experimental setup. In all cases, two K-type thermocouples were installed at the mold center and near the wall with their tips at 80 mm from the bottom of the mold to monitor temperature distribution of the bulk liquid during solidification. Solidification of the alloy continued up to the point where the melt temperature at the center of the billet reached 593 ± 2 °C. It is expected to have a solid fraction of 0.3–0.35 at this temperature according to equilibrium lever rule and Scheil's equation [4]. The wall temperature was registered at 591 ± 1 °C. After preparation, the billets were taken out of the mold, still in the mushy zone, and quenched quickly in cold water. For metallography, transverse section at the tip of the thermocouples was used and for consistency, the area between the center and the wall (quarter area) was examined.

4.1.1.2 Rheocasting, SEED Technology

In addition to low pouring process, the solidification behavior of billets produced via SEED technology was examined in detail. For these series of tests, about 2 kg of the alloy was poured into the same mold as explained in Sect. 4.1.1.1. For turbulence reduction during pouring, the mold was tilted during initial stage of pouring and was brought back to the vertical position (Fig. 4.4). Immediately after pouring the mold and its content were swirled at 150 RPM or 2.5 Hz with an eccentricity of 12 mm. The swirling motion is expected to not only distribute the solid particles formed on the mold wall, but also to break the dendrite arms and rendering the formation and uniform distribution of spherical particles. The duration of this stage depends on the mold dimension and the charge mass and for these series of experiments it was set to 60 s.

In the next step and after stopping the swirling motion and pausing for a short time (5–10 s), the bottom plug was opened to allow a portion of the residual liquid

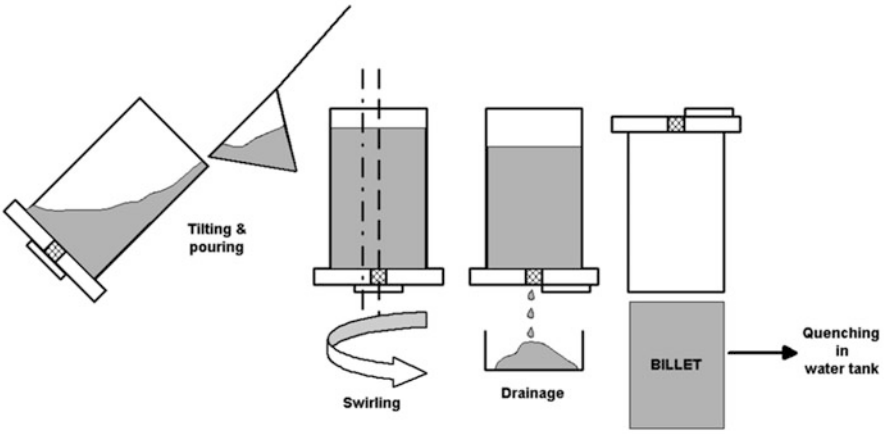

Fig. 4.4 Experimental procedure for the SEED process

to drain out. As a result, the fraction solid in the billet (slug) increases and a free-standing billet is produced. After a specific time of 20 s, the prepared billet was unloaded and transferred into the water tank to be quenched to room temperature at about 20–25 s. In all experiments, two 0.8 mm diameter K-type thermocouples were inserted near the mold wall and also the center with their tips at a distance 80 mm from the bottom of the mold to collect thermal data. The quenching temperatures for all the tests were 598.5 ± 2.5 °C. For metallography, transverse section at the tip of the thermocouples was used and for consistency, the area between the center and the wall (quarter area) was examined.

4.1.1.3 Electromagnetic Stirring (EMS)

For better understanding of the effect of stirring on the solidification behavior and resulted microstructure of SSM billets, electromagnetic stirring method was used. Binary Al–7%Si alloys were prepared by melting 99.7 % commercially pure aluminum in a SiC crucible in an electric resistance furnace. Addition of silicon and iron was carried out at 720 ± 5 °C using pure silicon and Al–25%Fe master alloy. The chemistry is given in Table 4.1.

For attaining different cooling rates, two dissimilar mold materials were used. For higher cooling rate, a copper mold with a water cooling jacket (Fig. 4.5b) and for the lower cooling rate, CO_2-bonded silica sand mold was used to produce ingots of 76 mm in diameter and 300 mm long. The entire configuration was placed in EMS machine, Fig. 4.5. For these series of experiments, the frequency was set to 50 Hz and the current was 100 and 30A for copper and sand molds, respectively (stirring was stopped around 400 °C in EMS samples).

For the superheat variation, pouring temperature was changed between 630 and 690 °C. The cooling rate above liquidus in the copper and sand molds for the

Table 4.1 Chemical analysis of the melt (wt. %)

Si	Fe	Al
6.7–6.9	0.8–0.81	Bal.

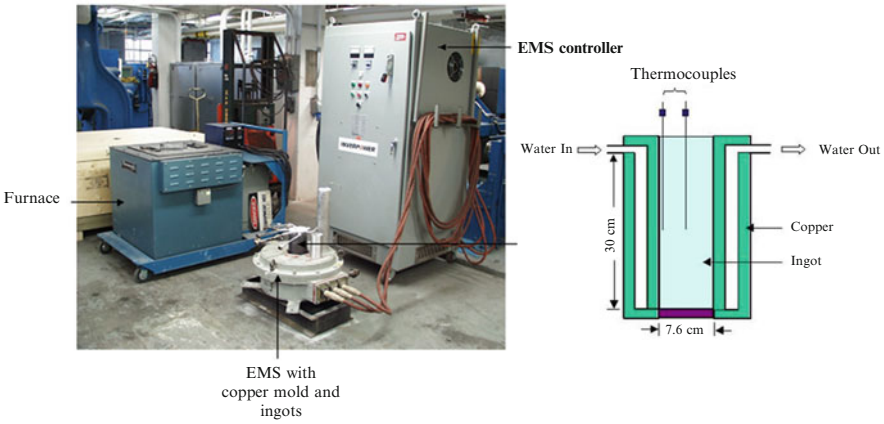

Fig. 4.5 (**a**) Setup for EMS experiments, (**b**) schematic details of the water-cooled copper mold

conventional ingot (with no stirring) was about 4.8 °Cs^{-1} and 3.3 °Cs^{-1}, respectively (thermocouples were inserted 200 mm from the bottom). The cooling rate in the sand mold is relatively high at the beginning of the pouring which is due to the large volume of sand compared to the liquid metal. However after the initial rapid heat dissipation, the bulk liquid temperature decreases slowly due to low heat diffusivity of sand mold. As a result, the sand could absorb significant amount of heat after filling the mold. The cooling rate is then reduced in the mushy zone. For the experiments with no stirring, the liquid was poured into the same molds and allowed to air cool. The samples with no stirring will be referred as "*conventional*." For structural study, samples were sectioned 200 mm from the bottom and the area between the center and the wall (quarter area) was examined.

4.1.1.4 Thixocasting of Refined/EMS Specimens

In addition, a limited number of experiments were carried out to study the solidification behavior of thixocast billets. For this purpose, graphite cup samples with ~25 mm diameter and samples from transverse section of EMS billets (200 mm from the bottom, in areas between center and wall) were reheated in a single coil 5 kW induction furnace operating at 80 kHz, Fig. 4.6 [6].

Samples were placed vertically on an insulator plate. Temperature variation during the tests was monitored by putting two thermocouples in the same manner as described in Fig. 4.1. Induction furnace was controlled by central thermocouple and the wall thermocouple was connected to the data logger system.

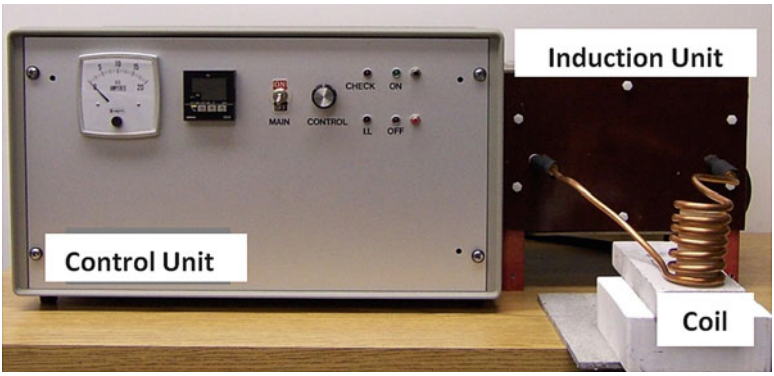

Fig. 4.6 Experimental setup for reheating of samples

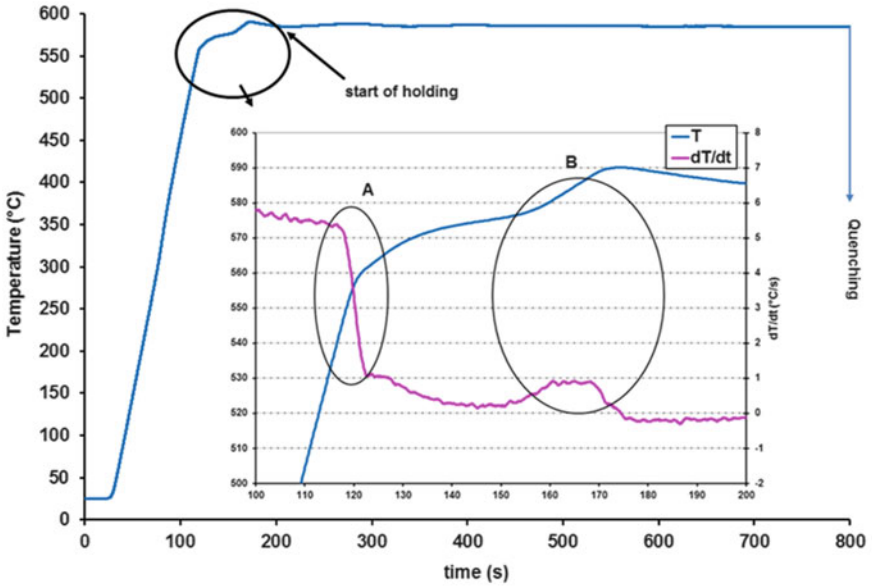

Fig. 4.7 Typical reheating profile of wall thermocouple

A typical reheating curve during partial remelting is presented in Fig. 4.7. During the tests, it was ensured that the temperature difference between center and the wall is less than 2 °C. Heating rate was set to 5–6 $°Cs^{-1}$ and reheating range was 583 ± 3 °C (about 38–40 % fraction solid according to ThermoCalc[1] calculations). Initial heating rate was rapid (5–6 $°Cs^{-1}$) while there is a sudden change in

[1]ThermoCalc is a commercial thermodynamic-based software package (www.thermocalc.com)

the slope of the curve (region A in Fig. 4.7) which is associated to the initiation of the sample remelting (by remelting of Mg_2Si constituent and ternary eutectic [1]). This variation is followed by another transformation due to the main eutectic reaction in region B of Fig. 4.7. After predetermined holding time (e.g., 5 or 10 min), samples were rapidly quenched in cold water.

4.1.2 Melt Treatment

The solidification behavior of SSM alloys is expected to change with the application of grain refining and modification treatments. The followings explain sample preparation and test procedures to characterize solidification behavior of melt-treated SSM billets.

In this study, three refiners and one Sr-based modifier with the following specifications were used:

- Al5%Ti1%B, rod form
- Al5%B, rod form
- Al4%B, waffle form
- Al10%Sr, rod form

To achieve different degrees of refinement, modification, and combined effects, the above-mentioned master alloys were added to the melt to raise the concentration of specific elements, i.e., Ti, B, and/or Sr levels in the alloy. Specified amount of these master alloys, wrapped in aluminum foil, were added to the melt between 720 and 730 °C using a preheated graphite bell. The entire melts were degassed with argon after master alloys addition and the contact time for the first sampling was set to 20–30 min depending on the treatment (~30 min for modification due to incubation period and ~20 min for sole grain refiner). Prior to taking any samples and after each step, each melt was cleaned by skimmer.

4.1.3 Chemical Analysis

Samples for chemical analysis were cast into a standard scissor mold. Disk shape samples having a 56 mm diameter and 10 mm thickness were prepared for chemical analysis by machining of the surface. Finally, 6–8 point OES ablations (Optical Emission Spectroscopy) were performed on the machined surface using ThermoARL-4460 and the results are presented by averaging all ablations. The measurement of the grain refiner and modifier elements concentrations is essential and thus calibration of the OES detector regarding these elements especially boron is vital. Two standards especially produced for analysis of 356 Al–Si alloys were used with a 1 % accuracy of the results. Table 4.2 shows the chemistries used in this book.

Table 4.2 Chemical composition of the base alloys (wt. %)

	Si	Mg	Fe	Mn	Cu	Ti	B	Sr	Al
Binary alloy	7.0–7.3	Nil	Max 0.09	Nil	Nil	Nil	Nil	Nil	Bal.
	6.7–6.9	Nil	0.8–0.81	Nil	Nil	Nil	Nil	Nil	Bal.
A356	6.4–6.7	0.36–0.4	Max 0.08	Max 0.003	Max 0.001	Max 0.0058	Nil	Nil	Bal.
356	6.8–7.0	0.33–0.36	Max 0.09	Max 0.003	Max 0.002	0.1–0.13	Nil	Nil	Bal.

4.2 Rheological Characterization

The flow of SSM billets within the die is an important issue to control the integrity of the finished cast product. Therefore, it is essential to characterize SSM billets flow when injected into die cavity. The following explains briefly the fundamentals of rheology and gives some equipment and procedures applied to complement the theoretical principles.

4.2.1 Principles of Rheology

4.2.1.1 Introduction

Since the inception of Semi-Solid Metal (SSM) processing concept in early 1970 [7, 8], and the fact that the deformability of SSM billets is shear rate and time dependent, the issue of rheology has been studied to some extent. The "S2P" biannual international conferences over the last two decades, (1990–2016) have also dedicated specific chapters covering rheological behavior of SSM alloys. Rheology is an integral part of SSM research efforts, even though the concept may not be as clear and familiar for metallurgists.

Rheology is the science of deformation and flow of materials. It is a branch of physics concerned with the mechanics of deformable bodies. It also deals with the simultaneous deformation and flow of materials. In this context shear flow is an important type of deformation in rheology and may be visualized as a process in which infinitely thin, parallel planes slide over each other as in a pack of rigid cards. The breakup or rupture of solids and liquids into smaller segments or droplets and the rejoining and sticking together, "*cohesion*," of particles or droplets to make a continuum body and mass are often included in rheology [9].

The rheological behavior and properties of a substance may sometimes exhibit considerable changes with time or with continuing deformation [10]. These changes occur either reversibly or irreversibly with reversible deformation called elasticity and irreversible deformation is known as flow. The work used in deforming a perfectly elastic body is recovered when the body is restored to its original

undeformed shape, whereas the work used in sustaining flow is dissipated as heat and is not mechanically recoverable. Elasticity relates to mechanically recoverable energy and viscous flow to the conversion of mechanical energy into heat. Elastic deformation is always a function of stress, whereas the rate of deformation for flow is a function of shear stress.

From the rheological point of view, the mechanical properties of material can be described in terms of elastic, viscous, and inertial contributions. For elastic deformation, the material deforms reversibly and is able to recover instantly to its original shape and size when the applied stress is removed. For viscous body however, stress and resulted strain cannot be sustained for long and will be relieved by flow with rate of flow being a function of stress. Of course, extremely viscous materials may exhibit elastic strain for considerable period of time. Periods which are short with respect to the time needed for appreciable flow. This means that a given material may be considered as an ideal elastic body for relatively short times and as an ideal viscous body for long time periods. Regardless of geometry of the body and deformation, the flow will always be in the form of laminar shear [11, 12].

With such simple definition, the interrelationship of rheology and mechanical properties of materials are closely tied up with materials' viscosity and deformation behavior within two phase region, liquid and solid, the so-called *mushy state*.

4.2.1.2 Viscosity

Viscosity is the main parameter for rheology of semi-solid metallic alloys and plays an important role equivalent to that of "fluidity" concept in liquid metals (e.g., [13–15]) and modulus of elasticity for solids [11]. Viscosity is an indication of SSM capability in filling the mold and determines the required force for deformation and flow of materials [16]. According to several review articles, viscometry is identified as an appropriate route for the rheological studies of materials [17–19].

Viscosity of fluids is expressed in terms of the coefficient of viscosity, η. Based on Newton's law of viscosity, the ratio of shear stress to the gradient of velocity is a constant showing the capability of momentum diffusion through the body of material as expressed mathematically in the following equation (4.2):

$$\tau_{yx} = -\eta \frac{\mathrm{d}v_x}{\mathrm{d}y} \tag{4.2}$$

Where $\frac{\mathrm{d}v_x}{\mathrm{d}y}$ is velocity gradient, τ_{yx} is the shear stress, and η is viscosity. Equation (4.2) may be rearranged and expressed as equation (4.3):

$$\tau_{yx} = -\eta \frac{-\frac{\mathrm{d}x}{\mathrm{d}t}}{\mathrm{d}y} = \eta \frac{\mathrm{d}x}{\mathrm{d}y} \times \frac{1}{\mathrm{d}t} = \eta \frac{\mathrm{d}\gamma}{\mathrm{d}t}$$

$$\tau_{yx} = \eta\,\dot{\gamma} \tag{4.3}$$

Where γ and $\dot{\gamma}$ are shear strain and shear strain rate, respectively. In contrast to Newton's law of viscosity where the viscosity (η) is constant, the term "apparent viscosity" is used when viscosity is influenced by applied shear rate.

The ratio of the viscosity, η, to the fluid density (4.4) is called *kinematic viscosity*, ν, which is a measure of momentum diffusivity, analogous to thermal and mass diffusivity [10]:

$$\nu = \frac{\eta}{\rho} \tag{4.4}$$

The value of η is interpreted in terms of a power law, relating shear stress (τ) to average shear rate, ($\tau = m\dot{\gamma}^{n}$). The apparent viscosity is then calculated as the ratio of shear stress to shear rate, [$\eta = m(\dot{\gamma})^{(n-1)}$], where m and n are material constants of consistency and power law indices respectively [10]. Except for Newtonian fluids where η is constant and the viscosity is independent of shear strain rate, the viscosity is found to vary by several orders of magnitude with changing shear rate (or shear stress) in non-Newtonian fluids, i.e., $\eta = \frac{\tau_{yx}}{\dot{\gamma}}$ is a function of $\dot{\gamma}$. Typical flow curves for non-Newtonian fluids are presented for time-independent fluids in Fig. 4.8 [10, 20]. Line A in this figure represents the Newtonian body for which η is constant. When the shear rate increases more than in proportion to shear stress, curve B, the material is called "*Pseudoplastic*" or "shear thinning" liquid. To a first approximation, the flow curve of a Pseudoplastic liquid can be represented by the power law, the rate of shear is roughly proportional to the power of the shearing stress or vice versa, (4.5 and 4.6):

$$\tau_{yx} = \eta(\dot{\gamma})^{n} \tag{4.5}$$

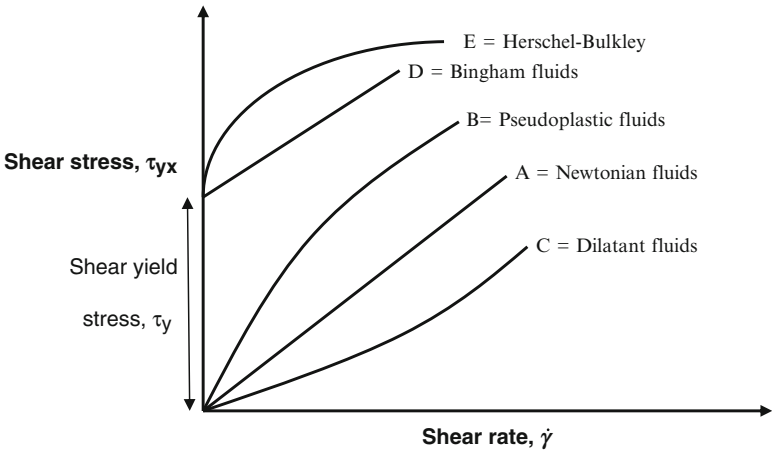

Fig. 4.8 Stress–strain rate curves for time-independent fluids (reproduced from [10] and [20])

$$\eta = m(\dot{\gamma})^{(n-1)} \tag{4.6}$$

The materials constants m and n (the consistency and power law indices, respectively [21]) are viscosity at shear rate of 1 s^{-1} ($m = \eta$) and a measure of fluid departure from Newtonian fluid ($n = 1$), respectively, i.e., $n < 1$ for pseudoplastic fluid (it is usually lies between 1/3 and 1/2, shear thinning) and $n > 1$ for dilatant fluid [10] or shear thickening.

It has to be mentioned that some of the non-Newtonian fluids may exhibit dual behavior, where both, shear thinning and shear thickening (pseudoplastic and dilatant, respectively) may be observed at different loading conditions. It has been reported that aluminum and tin–lead alloys have shown both the pseudoplasticity and dilatant behaviors depending on the applied shear rate when tested with high pressure die casting setup and rotational viscometer. Such alloys behave like pseudoplastic material at low shear rates, 2×10^3–2×10^4 s^{-1}, but show dilatant character when deformed at high shear rates, 10^6 s^{-1} [22, 23].

In addition, there are viscoelastic fluids which exhibit time-dependent recovery from deformation, i.e., recoil. This is in contrast with the behavior of Newtonian fluids which do not recoil. Such behavior may be compared with the behavior of thermoplastic polymers under loading with exception of elastic deformation which is due to stretching (straightening) of the polymer chains, instantly happens as load applied and is recovered instantly when load removed, ε_i in Fig. 4.9. After chain straightening, the chains start to move relatively with respect to each other and this is time dependent as is the case for viscoelastic fluids with layers of fluid moving with respect to each other. Such movement of chains or layers of fluid with respect to each other is known as "*viscous flow*" and therefore, viscoelastic deformation ($\boldsymbol{\varepsilon_f - \varepsilon_i}$) is time dependent. Viscous flow, however, is dependent upon the viscosity. Such characteristic brings the time dependency of viscosity into the actual fluids.

The semi-solid materials with their thixotropic characteristics, as will be discussed later, do not store elastic energy and therefore do not recover with time when the applied shear stress is removed. The viscosity of thixotropic fluids decreases with time and approaches an asymptotic value at a constant shear strain rate and also the structure breaks down with time. As pointed out by Poirier and

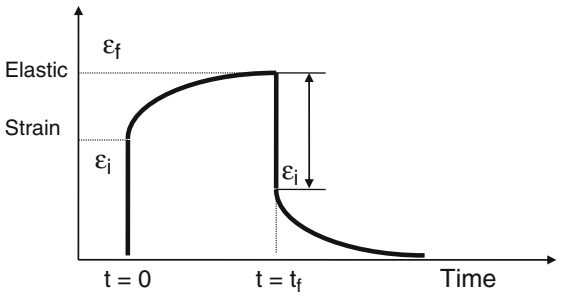

Fig. 4.9 Strain-time variation for viscoelastic deformation of polymers. For fluids, the recovery of instant elastic deformation is not applicable [24]

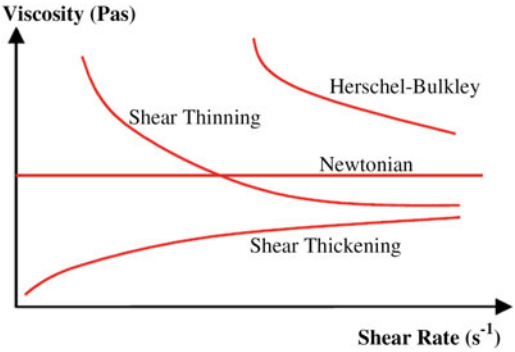

Fig. 4.10 Effect of shear rate on viscosity of different fluids [20]

Geiger [10], thixotropic fluids may be treated as general Newtonian fluids under steady-state conditions when the asymptotic value of viscosity is maintained.

The Bingham fluids exhibit a yield stress and then gives a linear relationship between shear stress and shear rate as expressed in (4.7)[20]:

$$\tau = \tau_y + k\dot{\gamma} \tag{4.7}$$

where τ_y is yield stress and k is a constant related to the viscosity. However, if the fluid behavior after yielding is not linear, it is referred as Herschel–Bulkley fluids where (4.8):

$$\tau = \tau_y + k\dot{\gamma}^n \tag{4.8}$$

Figure 4.10 represents viscosity variations against shear rate for different fluids [20]. In the eyes of mass producers of metallic artifacts, knowledge of viscosity is equivalent to die-filling characteristics, since lower viscosity causes better movement of material through the die [22, 25, 26]. The viscosity is always used as an input parameter for prediction of flowability in the simulation software [27–29]. Lower viscosity results in intricate thin wall component production with lower machine pressure and reduced rejects and scraps [30, 31].

4.2.1.3 Flow Behavior in the Semi-Solid Metals

The semi-solid metals are two-phase system containing a suspension of primary phase particles within the liquid phase matrix. The dynamic presence of two phases, "*the mush*", is dependent upon the alloy solidification range where a wider solidification range is translated into an easier and more controllable "*mush*". The growth mode of the solid phase is dendritic. Such system is shown to behave like Newtonian or non-Newtonian fluids depending upon the process parameters [17–19].

Semi-solid metal slurries with globular morphology of the solid phase and a solid fraction of less than 0.6 usually exhibit two distinct rheological characteristics: thixotropy and pseudoplasticity [19]. Thixotropy is about the time dependency of the transient state viscosity at a given shear rate, while pseudoplasticity discusses the dependency of the steady-state viscosity on the shear rate. All the SSM processing techniques rely on either one of these properties or both in a single process. Therefore, a good understanding of the rheological behavior of SSM slurries is mandatory to develop effective SSM processing technologies. The rheological phenomena in stirred SSM slurries can be divided into three groups [7, 32, 33]:

1. Continuous cooling behavior, which describes the changes in the viscosity of molten alloy during continuous cooling (at constant cooling rate and shear rate).
2. Pseudoplastic behavior, which describes the dependency of steady-state viscosity on the shear rate, or shear thinning behavior.
3. Thixotropic behavior, to describe the dependency of transient state viscosity on time.

There is important information that could be obtained on the rheological behavior of SSM slurries during continuous cooling with respect to the effects of solid fraction, shear rate, and cooling rate. In particular, it is more relevant to the practical conditions set in SSM processing techniques such as rheocasting and rheomolding. However as pointed out by Suéry et al. [16], such experiments are more relevant to exploiting the solidification behavior rather than studying the rheology of SSM slurries.

In contrast to continuous cooling tests, isothermal steady-state trials are more capable of characterizing the rheological behavior of SSM slurries and are a first step toward the determination of a constitutive equation. It is now generally accepted that the steady-state viscosity at a given shear rate depends on the degree of agglomeration between the solid particles, which in turn is the result of a dynamic equilibrium between agglomeration and deagglomeration processes [34].

The thixotropic behavior of SSM slurries was demonstrated by measuring the hysteresis loops during a cyclic shear deformation [35]. However, such procedure is not sufficient to quantify the kinetics of agglomeration and deagglomeration processes. As pointed out by Chen and Fan [34], in order to overcome this shortcoming, special experimental procedures involving an abrupt shear rate jump or a shear rate drop were developed to characterize the kinetics of structural evolution. It was found that the agglomeration process dominates after a shear rate drop, whereas a deagglomeration process dominates after a shear rate jump [34].

For the semi-solid billets with high fraction solid, the so-called self-standing slugs, there are other type of rheological studies which are based on keeping the shear rate constant within the bulk of a preheated sample and measuring the velocity of deformation under a constant dead weight, parallel plate compression viscometry, or deals with constant stress applied on the semi-solid slugs to develop the data of strain rate, extrusion methods. Such data can provide useful information about the viscosity of SSM materials having high percentage of fraction solid [36–38].

4.2.2 Rheological Behavior of SSM alloys

The flow and deformation of metallic alloys "rheological behavior" is mainly dependent on the SSM alloy viscosity (η), which itself varies with both metallurgical and process parameters. It may be represented by the following (4.9) [33, 34, 39, 40]:

$$\eta = f(\dot{\gamma}, t_s, T_a, \dot{T}, C_o, f_s, F, h_{\text{istory}}) \tag{4.9}$$

Where η represents the viscosity, $\dot{\gamma}$ is the shear rate, t_s is shearing time, T_a is the temperature of semi-solid alloy, $\dot{T}$ is the cooling rate from liquid to T_a within the mushy zone, C_o is the alloy composition, f_s is fraction solid at T_a, F is the shape factor, and h_{istory} is history effect. Generally higher solute contents and cooling rates have been found to cause more dendritic morphology and hence higher viscosities for a given fraction solid. The apparent viscosity of the slurry at a particular point in time depends on its previous internal state (the history effect, h_{istory}). The internal state, which is continually changing, is described in some way by microstructural parameters such as size, size distribution, morphology, and dispersion of solid phase within the liquid matrix. Developing an all-encompassing model for semi-solid metals is therefore considered to be a difficult task and requires detail knowledge of the effect of the above-mentioned parameters on the viscosity. In addition, the process time before shaping is also important since it could change particle size, morphology, and distribution due to spheroidization and coarsening [41, 42]. The followings give a brief account of the effects of parameters on the viscosity of SSM slurries.

4.2.2.1 Metallurgical Parameters

The complex rheological properties of SSM alloys are strongly dependent on the local solid fraction, particle shape, and size and the state of agglomeration. The metallurgical parameters may be controlled through manipulation of solidification and alloy phase diagram.

Fraction Solid

One of the most important parameters affecting viscosity of the mush is the fraction solid of the primary phase, e.g., α-Al dendrites in case of Al–Si alloys [38, 43–45]. Fraction solid ($f_s = 1 - f_l$) at a temperature T within mushy zone may be calculated by Scheil equation, (4.10) and (4.11) [4].

The fraction solid (f_s) at a given location within the solid–liquid zone is predicted by a mass balance wherein a simplest case neglects ripening and diffusion in the solid. For this case the relation between weight fraction liquid in mushy zone,

f_l, and liquid composition at a given location, C_l, is given by the Scheil equation which may be written in the following form for the constant partition ratio, k:

$$f_l = \left(\frac{C_l}{C_o}\right)^{-1/1-k} \tag{4.10}$$

Or for fraction solid and solid composition (C_s) is given by:

$$C_s = kC_0(1 - f_s)^{k-1} \tag{4.11}$$

C_0 is the composition of the alloy.

Different methods are reported in the literature for measuring the fraction solid, among which the most commonly used are quantitative metallography, thermal analysis, and application of thermodynamic data based on equilibrium phase diagram [46]. Each route has its advantages and disadvantages and could be used as per requirements of the research program.

Chen and Fan [34] developed a microstructural model to describe the relationship between viscosity and effective solid fraction, rheological behavior, of liquid-like SSM slurries under simple shear flow. In their model, liquid-like SSM slurry is considered as a suspension in which interacting spherical solid particles of low cohesion are dispersed in a liquid matrix. In a simple shear flow field, a structural parameter (S) defined as the average number of particles in each agglomerated solid particle was used to describe the state of agglomeration and deagglomeration. Through effective solid fraction, f_s^{eff}, a parameter which is slightly different to that of fraction solid as a result of agglomeration/deagglomeration and possible entrapment of liquid, (4.13), viscosity can be expressed as a function of the structural parameter S (4.12).

$$\eta = \eta_o\left(1 - f_s^{\text{eff}}\right)^{-\frac{5}{2}} \tag{4.12}$$

The effective fraction solid is given as:

$$f_s^{\text{eff}} = \left(1 + \frac{S-1}{S}A\right)f_s \tag{4.13}$$

where η is instantaneous viscosity, η_o is the viscosity of liquid matrix (when effective fraction solid = 0), A is a model parameter related to packing mode which decreases with increasing the packing density (the fraction of space filled by solid particles). The parameter A was expressed by a linear equation of ($A = 3.395–4.96\ f_s$, where f_s = solid fraction) for Sn15%Pb alloy [47], and the effective fraction solid $\left(f_s^{\text{eff}}\right)$ was regarded as the sum of the actual solid fraction and entrapped liquid fraction.

Equation (4.13) indicates that the effective solid fraction is influenced by the actual solid fraction, agglomerate size, and the packing mode in the agglomerated

chunks. It is interesting to note from (4.12) that the viscosity of semi-solid slurry is a direct function of the viscosity of the liquid matrix and the effective solid fraction. The flow conditions affect viscosity only indirectly through changing the effective solid fraction.

Viscosity steadily increases with increasing of solid fraction till the point where solid particles can no longer move easily and the already solidified segments have developed strength, a 3D solid skeleton is formed. This is specified as the dendrite coherency point (DCP). The dendrite coherency point marks the transition from mass feeding to interdendritic feeding during solidification. After DCP, viscosity increases abruptly [48].

With stirring in SSM processing, dendrite coherency point is postponed due to the shallow temperature gradient initiated from the forced convection within the melt. The breakdown of dendrites due to stirring coupled with multidirectional growth of fragmented dendrites due to more uniform temperature distribution within the mold, shallow temperature gradient, encourage the formation of equiaxed grains, thus postpone the rapid rise of viscosity to higher fraction of solids.

The effect of fraction solid was studied on the viscosity of A356 SSM billets cast conventionally [38]. Application of low superheat in conventional casting resulted in the formation of the desired primary Al morphologies for a series of SSM billets. It was confirmed that at low shear rate values (less than 0.01 s^{-1}), the SSM billets can be treated as the Newtonian fluid even though the two-phase fluids are basically non-Newtonian with engineering strain–time behavior comprising non-steady-state or transient state with thixotropic characteristics and quasi-steady-state from which the viscosity values calculated [38]. The SSM billets showed pseudoplastic behavior where the viscosity numbers decreased with increasing applied pressure (shear rate) as shown in Fig. 4.11. The SSM billets were also treated as the non-Newtonian fluids and the materials constants m and n were calculated and presented as an empirical relationship (4.14) for different fractions solid [38].

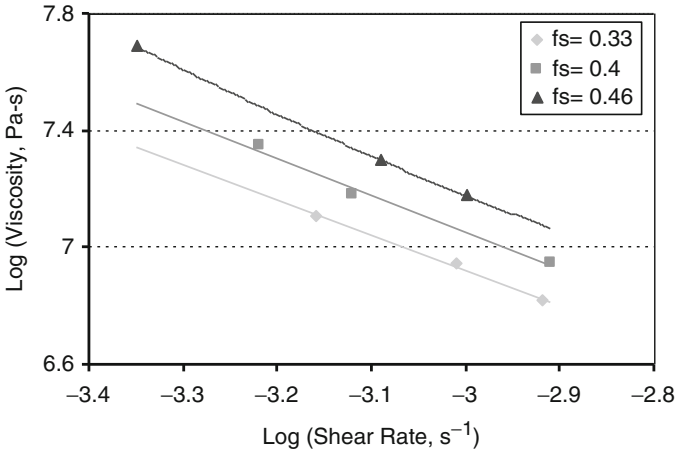

Fig. 4.11 The viscosity numbers are plotted against average shear rates for SSM billets having different fractions solid [38]

$$\log \eta = 5.56 - 1.39 f_s - (1.56 f_s + 0.14) \log \dot{\gamma} \quad (0.33 < f_s < 0.46) \tag{4.14}$$

The above-mentioned empirical relationship expresses the direct effect of fraction solid on the viscosity of semi-solid billets and if the fraction solid kept constant, the viscosity varies inversely with shear rate. The validity of equation (4.14) was further confirmed with experimental results reported in the literature and it was stated that the equation above is valid at very low shear rates, less than 0.01 s^{-1} [38].

Primary Phase Morphology

The morphology of primary phase has a pronounced effect on the flow behavior of semi-solid metal slurries [17–19]. It is found that dendritic structures at the same solid fraction exhibit approximately several orders of magnitude greater flow resistance than the equiaxed structures [49]. In fact the globular particles move easier over one another than dendritic ones which tend to interlock during the application of external force, resistance against flow [7, 33, 50, 51]. In addition, since the beginning of SSM processing research, it was the nondendritic structure which imparted the interesting and useful rheological characteristics, such as pseudoplasticity and thixotropy. Therefore, a good understanding of the effect of particle morphology on the rheological behavior is not only of scientific merits but also from technological point of view it has great significance on the development of new SSM processes.

Although several attempts were made to experimentally correlate the morphology of the primary solid phase to rheological characteristics (e.g., [37, 52]), there is not any theoretical model to account for the effect of particle morphology on the flow behavior of metal slurries. However, there are simple models and defined parameters to describe rheological characteristics of slurries with different solid particles morphologies [50]. Lashkari et al. [37] specified the effect of morphology on flow characteristics of SSM billets using aspect ratio of the primary α-Al particles in Al–Si hypoeutectic alloys. Non-Newtonian behavior for SSM billets was assumed and non-Newtonian power law model was employed to study rheological behavior of SSM slurries. The model expresses viscosity changes in terms of applied stress and resulting shear rates as (4.15):

$$\eta = m(\dot{\gamma})^{n-1} \tag{4.15}$$

where, as mentioned before, m and n are the material constants (consistency and power law indices), respectively [21]. Figure 4.12 shows the relationship between the consistency and power law indices and aspect ratio which eventually related to viscosity of SSM slurries. The relationships between n and m with aspect ratio are given as (4.16 and 4.17):

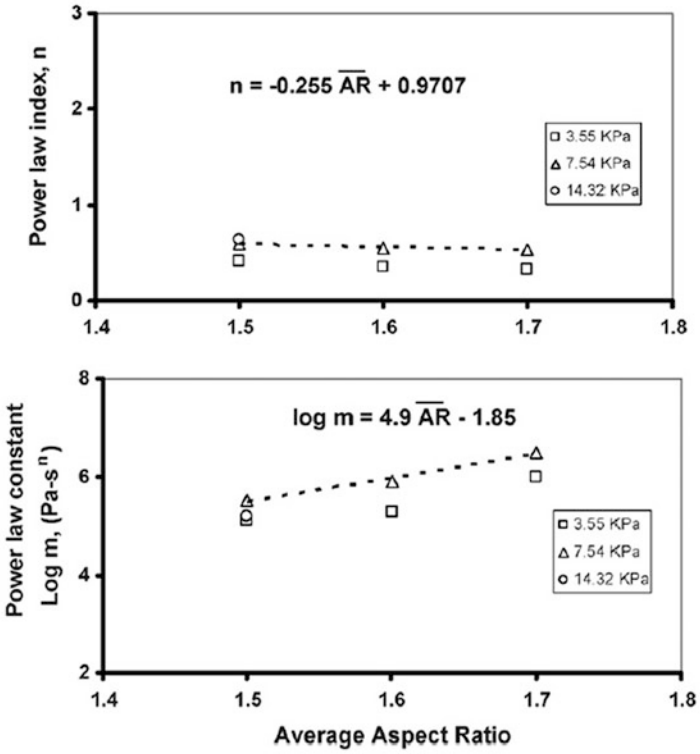

Fig. 4.12 Effect of primary α-Al particle aspect ratio on the power law (n) and consistency (m) indices [37]

$$n = 0.97 - 0.255\left(\overline{AR}\right) \quad \text{for } 1.5 < \overline{AR} < 1.7 \tag{4.16}$$

$$m = 10^{\left(1.85 - 4.9\,\overline{AR}\right)} \quad \text{for } 1.5 < \overline{AR} < 1.7 \tag{4.17}$$

In another study [19, 50], Fan and his coworkers studied the effect of morphology on the apparent viscosity (the viscosity of steady-state flow segment) of SSM slurry using the concept of fractal dimension, D_f. Fractal dimension defined as the parameter to characterize the morphology of solid particles using the concept of Hausdroff dimension. Hausdorff dimension of a single point is zero, of a line is 1, of a square is 2, and of a cube is 3. For dendritic morphology, the value of $D_f = 2.5$ and $D_f = 3$ illustrates the fully globular particles in SSM slurries.[2] They calculated D_f from experimental viscosity data of continuous cooling experiments on Sn–15 % Pb [35]

[2]For more information on fractal dimension, interested readers are encouraged to consult the following article;

R.S. Qin and Z. Fan, "Fractal theory study on morphological dependence of viscosity of semisolid slurries", Mater. Sci. Tech., 2001, 17, 1149–1152.

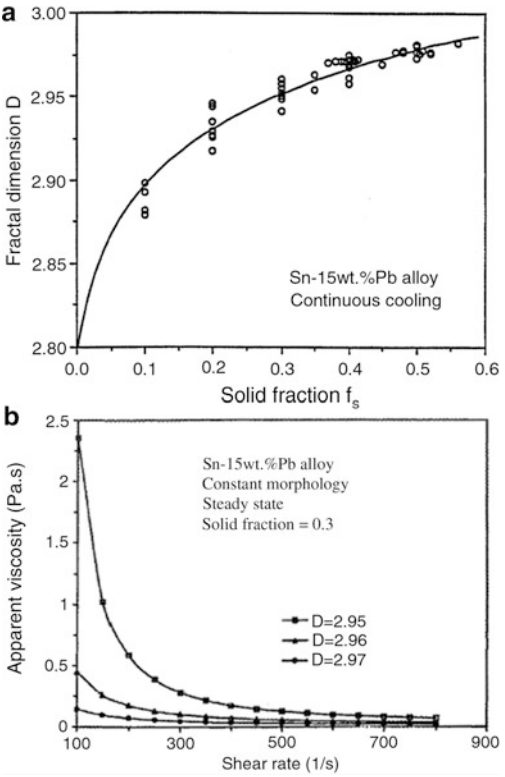

Fig. 4.13 The effect of primary particle morphology on the apparent viscosity as a function of shear rate; (**a**) Fractal dimension D deduced from experimental viscosity data from continuous cooling experiments reported by Joly et al. [35] as function of solid fraction [19], (**b**) calculated steady-state apparent viscosity at three different fractal dimension values for Sn15%Pb SSM alloy [50] (reprinted by permission of Taylor & Francis Ltd)

as shown in Fig. 4.13a and substituting the resulted values in (4.13) and (4.12) to calculate the effective solid fraction and apparent viscosity, respectively, Fig. 4.13b. As shown, for D_f value closer to 3, the apparent viscosity is lower [50].

Zoqui et al. [53] also reported the effect of morphology on the rheology of SSM alloys, using rheocast quality index. Rheocast quality index, RQI, defined as RQI = globule size/(grain size × shape factor), indicates quasi rosette shape feature with RQI = 0.1 and a perfect globular shape with RQI = 0.9.

Particle Size and Distribution

One of the main parameters controlling the complex rheological properties of semi-solid metal alloys is the particle size and distribution including the state of agglomeration. It is expected to have better flow with finer microstructure as there is easier movement and less collision among particles with lower viscosity [17–19].

It has to be pointed out that finer particles are prone to agglomeration due to larger surface area and therefore there may be changes in viscosity with time, dynamic state. Generally, size and distribution of primary particles are time-dependent variables based on two mechanisms of breakdown (deagglomeration),

and coagulation (agglomeration) [54, 55]. For the breakdown mechanism (deagglomeration process), the bonds between particles break down due to shear forces during the early stages of the shearing and is responsible for the rapid decrease in the effective viscosity of the material [56, 57]. The second mechanism is the buildup of the solid structure where metallurgical bonds (necks) form between particles when the sample is at rest [57, 58]. It is understandable that the first mechanism is much faster than the second since the agglomeration mechanism relies on diffusion which is not as effective and fast as stirring and generation of convective currents during deagglomeration. The tendencies for the suspended particles within the liquid matrix to agglomerate could be decreased or increased with the application of external forces on the semi-solid mush.

The particle size is therefore dependent on the applied shear rate as it can promote agglomeration or deagglomeration due to particle–particle impact and bonding if the applied shear rate is low. It is also time dependent during isothermal processing of SSM billets where Ostwald ripening (dissolution of smaller particle and growth of larger ones) or particles coalescing (particles joined together by impact and due to high diffusion rate fully fuse together) could change particle size. Therefore, the dynamic interaction among solid particles may cause the formation of chunks, agglomerated particles, within semi-solid slurries and make the flow of mush harder. However, after a while under the influence of viscous forces, the equilibrium takes place between agglomeration and deagglomeration processes and the viscosity changes reach a steady state and uniform distribution of particles is observed [33, 47, 50, 51, 59, 60]. The uniform distribution of isolated particles within semi-solid slurries is always an important issue for researchers to lower viscosity and achieve sound final components.

Particle size analysis and distinction between grains and globules have paramount importance in SSM processing. Technically, there is a difference between globule and grain sizes. Globules are the primary particles which are apparently detached from each other; however, there is every possibility that the neighboring individual particles might be interconnected from underneath of the polished surface. It is worth noting that the concept of globule size measurement in conventional cast samples is not scientifically valid which is associated with the errors related to the sectioning of dendritic branches. This will be explained later in this chapter.

Alloy Chemistry and Pouring Temperature

Alloy Chemistry

The composition of slurry has a direct effect on the solidification morphology. Increasing solute concentration in the alloy causes enrichment of melt at the solidification front. The resulting constitutional supercooling breaks down planar interface to cellular morphology which eventually becomes dendritic with increasing constitutional supercooling at the solidification front. With the formation of dendrites, as stated earlier, the apparent viscosity of slurry increases and rheocasting in this condition becomes more difficult.

It is believed the higher concentration of solute in the alloy increases the volume fraction of liquid trapped between the primary crystals. Such phenomenon brings higher viscosity within the slurry. An empirical equation has also been proposed to relate the viscosity and compositional factors [61, 62].

$$\eta = \eta_o \left\{ 1 + \frac{\alpha\rho\, C^{1/3}\, \dot{\gamma}^{-4/3}}{2\left(\frac{1}{f_s} - \frac{1}{0.72 - \beta C^{1/3}\dot{\gamma}^{-1/3}}\right)} \right\} \tag{4.18}$$

where η_o is the apparent viscosity of liquid, ρ is the density of alloy, C is the solidification rate $\left(\frac{df_s}{dt}\right)$ (fraction solid forms per unit time, t), f_s is the fraction of solid, $\dot{\gamma}$ is the shear rate, and α and β are numerical values which are dependent on the chemical composition of alloy and become larger with increasing solute content. For Al–3.6 % Si, the value of $\alpha = 67.0$, $\beta = 6.27$ and density (ρ) are 2140 kg m^{-3} [61].

Furthermore, alloy composition could affect dendrite coherency point (DCP), as it is altered by solute concentration [48]. This is due to the effect of solute concentration on the formation of the primary solid phase as, for instance, for hypoeutectic Al–Si alloys, the percentage of primary α-Al decreases with increasing Si content and therefore the development of dendritic network is postponed, lower dendrite coherency temperature.

The effects of solute and trace elements on reducing grain size and improving mechanical properties of as-cast products are well-established facts (see Sect. 6.2.1.4). The alloy composition directly affects the percentage of primary phase solidifying within mushy zone. It is generally believed that small addition of alloying elements could interfere with grains nucleation and growth mechanisms and provide conditions required for new nuclei to form or prevent gain coarsening, to promote the formation of finer grains. With progress in solidification, the solutes form an enriched boundary layer ahead of the solidification front in which the actual temperature is lower than the equilibrium solidification temperature, constitutional undercooling zone [4]. Constitutional undercooling is responsible for dendritic growth. In other words, with controlling alloy composition, the type and percentage of solute elements, constitutional undercooling and thus the growth rate and morphology of primary phase, dendritic or equiaxed growth, may be controlled. The same concept could be extended for grain refiners which are specifically added to refine the as-cast structure. The effect of grain refiner and modifier addition during SSM processing of aluminum alloys is well discussed in this book (Sect. 6.2.1). The overall conclusions may be briefly summarized here as follows:

1. Grain refinement results in the formation of better and more uniform distribution of nearly spherical primary α-Al particles within the slurry.
2. The refinement of the grains has been identified as the main factor for better deformability of the billets. Modification also plays an important role in alloy deformability through reduction of the residual liquid surface tension, which reduces the apparent viscosity of the billets.

3. The microstructural study of the deformed area showed less segregation of liquid adjacent to the mold walls for the combined and overrefined semi-solid billets. This is attributed to the smaller particles size and lower viscosity of the billets.

Pouring Temperature

Pouring temperature or superheat is one of the important parameters to affect the evolution of primary phase during solidification. Several researchers have investigated the effect of pouring temperature on the microstructure of as-cast semi-solid metals (e.g., [63–69]). Low superheat is instrumental in establishing shallow temperature gradient within the slurry, thus encouraging equiaxed growth. Shallow temperature gradient removes directional heat extraction from the melt and prevents the formation of columnar dendrites within the mush [4]. This is an effective way to control the morphology of primary phase forms in the more recently introduced SSM processes, since agitation of the slurry is no longer the principal factor in promoting globular morphology [25, 68, 69]. Figure 4.14 shows the effect of pouring temperature on the microstructural evolution of 356 Al–Si alloy [67].

The importance of pouring temperature is even well pronounced in SSM processes where stirring with strong convective currents is applied as in case of electromagnetic stirring route which will be discussed in Sect. 5.4.

4.2.2.2 Process Parameters

Shear stress and shear rate $(\tau, \dot{\gamma})$

One of the most important factors affecting the viscosity of SSM slurries is the applied shear force [39, 43]. It imposes laminar or turbulent flow within the slurry and induces disintegration of dendrites and the agglomeration or deagglomeration of the dendrite fragments, which is the main drive for fine distribution of primary phase particles. The applied shear force could eventually establish some sort of equilibrium between agglomeration and deagglomeration phenomena within SSM slurries, "steady state," and to prevent the formation of bulky particles; the main obstacle to SSM slurries flow within mold cavity. The great tendency for the formation of agglomerated chunky parts due to the presence of low energy grain boundaries within globular particles can be prevented by application of shear forces within the slurry [70]. The term "apparent viscosity" used for SSM slurries is to express the viscosity of steady-state flow and varies with shear rate and fraction of solid [7, 32]. As shown in Fig. 4.15, for a constant fraction solid, the viscosity decreases with increasing shear rate.

Shear rate is a material-related parameter which varies linearly with shear force in Newtonian fluids and nonlinearly in non-Newtonian fluids. Shear rate plays the same role as shear force where the increasing of shear rate decreases the viscosity within non-Newtonian fluids as shown in Fig. 4.11 and also Fig. 4.16. For ideal Newtonian fluids, the viscosity number is independent of shear rate [7, 32].

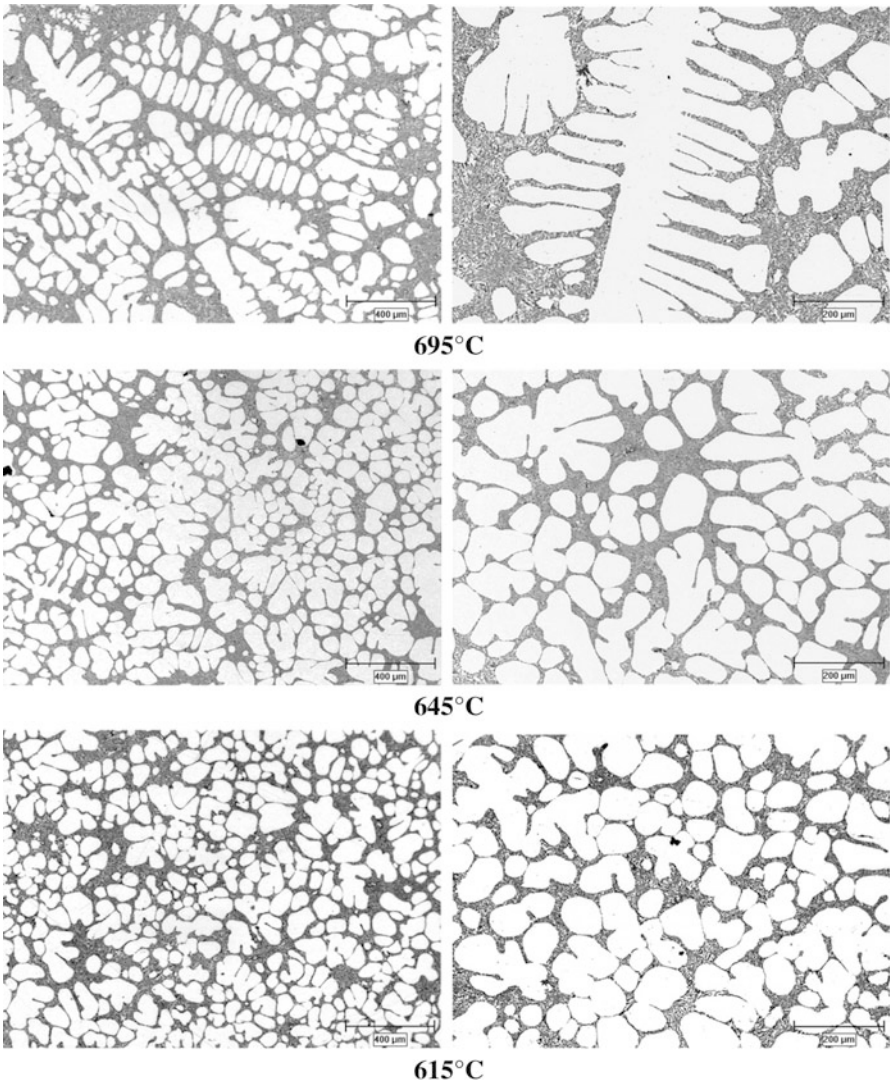

Fig. 4.14 Typical optical micrographs to show the effect of pouring temperature on the morphology of primary α-Al particles. Dendritic, rosette, globular (from 695 to 615 °C) [67]

The implementation of shear force and the resulting agitation of the slurry are brought about by different means which explained earlier in Chap. 2 for a range of SSM processes. Application of shear force also plays an important role during the course of preparing the primary feedstock for thixo- and rheo processes, where the mechanical rheocaster or agitator is the means by which the SSM billets are produced [71]. Swirling is another example of external force which not only induces shear stresses, but also brings thermal homogeneity within the SSM slurry

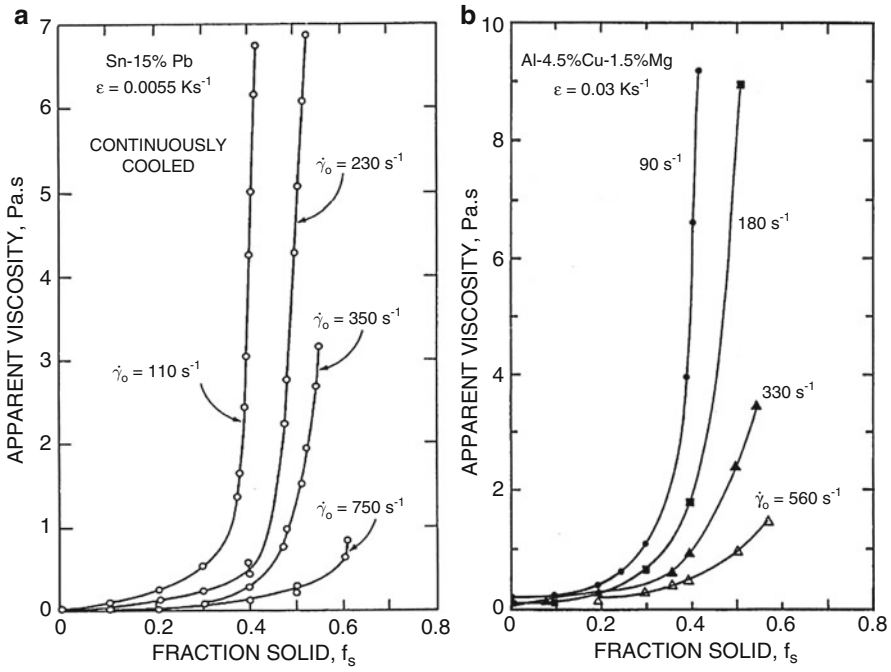

Fig. 4.15 Apparent viscosity versus fraction solid at different shear rates to confirm the viscosity decreasing with increasing shear rate, (**a**) Pb15%Sn [35] (**b**) Al4.5%Cu1.5%Mg [32]

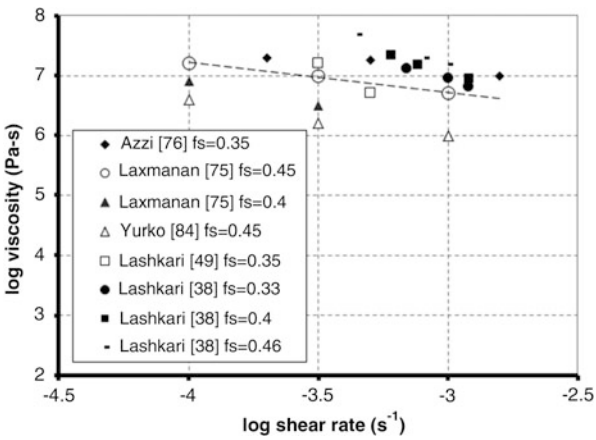

Fig. 4.16 The effect of shear rate on the viscosity of SSM slurries having similar fraction solid and globular morphology and tested within the same range of shear rates [38]

and establishes shallow temperature gradient to alleviate nucleation barrier within the bulk liquid. In addition, swirling may assist in disintegration of secondary and tertiary dendrites. Such phenomenon resulted in equiaxed grain growth in SSM cast billets with distinct deformation and flow characteristics (e.g., [72]).

Prasad et al. [73] have proposed a correlation (4.19) between particle size and fraction solid, cooling rate, and shear rate, which is in good agreement with experimental results. It is a useful tool to predict the effect of process parameters on the particle size.

$$d = \frac{\Phi D_l^{4/9}(T_l - T)^{1/3}}{\dot{T}^{1/3}\dot{\gamma}^{1/3}} \left(\frac{-f_s}{(1-f_s)\ln(1-f_s)}\right)^{1/3} \left(\frac{C_l - C_o}{C_o - C_s}\right)^{2/3} \tag{4.19}$$

where d is the particles diameter, D_l is liquid diffusivity, T_l is the liquidus temperature of the alloy, T is the temperature in the semi-solid region, C_o is the bulk liquid composition, C_l (4.21) is liquid composition at the interface, C_s (4.22) is the mean composition of the solid formed, $\dot{T}$ is cooling rate, $\dot{\gamma}$ is the shear rate, and f_s (4.20) is the fraction of solid. The value of Φ in (4.19) cannot be found from theoretical analysis as its value is dependent on the relationship between the fluid flow velocity and the velocity for particle–fluid slip. This relationship is not well defined, and therefore the value of Φ must be determined from the best fit of experimental data. However, Prasad et al. [73] pointed out that a detailed computer analysis of the experimental data suggested that for a Couette viscometer-type rheocasting system the empirical value of Φ can be taken as $\frac{0.119}{C_0^{2/3}}$.

$$f_s = 1 - \left[\frac{T_0 - T_l}{T_0 - T}\right]^{\frac{1}{1-k}} \tag{4.20}$$

$$C_l = \frac{C_0}{[1 - (1-k)f_s]} \tag{4.21}$$

$$C_s = \frac{C_0[1 - (1-f_s)/\{1 - (1-k)f_s\}]}{f_s} \tag{4.22}$$

where T_o is the melting point of the pure solvent metal and k is the solute partition coefficient.

Shearing time (t_s)

For constant shear rate tests, the changes of viscosity are dependent on the duration time of shearing. Based on the stirring time, the rheological behavior of SSM slurries may be divided into two stages of transient and steady state. In the transient state, the viscosity is a function of time but in the steady-state condition, viscosity is constant and is only proportional to shear rate [10].

In more detail, the dynamic interactions among the solid particles result in the formation of agglomerates. The newly formed agglomerates may collide together to generate newer agglomerates with even larger size under viscous forces. Parallel to agglomeration, the already agglomerated particles may also break up, deagglomerate giving rise to agglomerates of a smaller size. At a particular time, the degree of agglomeration between solid particles depends on the nature of the system including particle size, its volume fraction, and the external flow conditions.

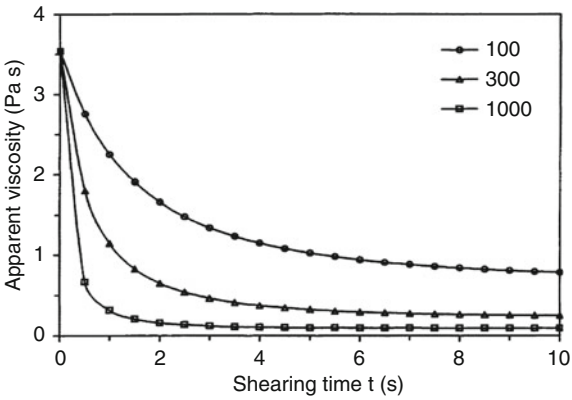

Fig. 4.17 Comparison of calculated transient state viscosity of Sn15%Pb alloy with solid fraction of 0.4 under different shear rates (s^{-1}) as function of shearing time [19] (reprinted by permission of Taylor & Francis Ltd)

At steady state, the degree of agglomeration is a direct result of the dynamic equilibrium between two opposing processes of structural buildup (agglomeration) and breakdown (deagglomeration) [59]. This condition is accessible after sufficient time from the beginning of shearing the slurry. But in transient state, which occurs at a time between the start of shearing and steady-state condition, there is not equilibrium between agglomeration and deagglomeration processes and the measured viscosity of slurry varies with time of stirring up to steady-state condition. The amount of transient time is dependent on the amount of induced shear force and decreases with increasing shear force. Other parameters such as shear rate can affect steady state and transient state conditions as seen in Fig. 4.17. It is clear that with increasing shear rate the slurry reaches steady-state condition at shorter time [19].

Cooling rate and holding temperature and time

Cooling rate, $\dot{T}$, shows the speed of heat extracted from slurry. It is well established that the magnitude of cooling rate has direct effect on the rate of solid formation or growth rate R. Increase of cooling rate causes increasing of growth rate and promotes dendritic solidification. The formation of dendrites and eventual dendritic skeleton increases the viscosity of slurry in comparison with the same fraction solid at lower cooling rate where the formation of a 3D skeleton is postponed. Figure 4.18 shows the effect of growth rate and temperature gradient on the solidification morphology of Sn–Pb alloy [4].

Holding temperature is the parameter to control the fraction solid in mushy zone. The relationship between the holding temperature and fraction solid may be determined by lever rule, Scheil's equation, thermal analysis, or microscopic examination of quenched specimens. It is clear that higher fractions solid cause greater viscosity values [40] as shown in Fig. 4.15. It is also apparent that higher shear rate values are needed to compensate for greater fractions solid if the viscosity remains the same [7, 32].

It is not easy to differentiate between the effects of temperature and fraction solid on the viscosity of slurries due to their intertwined close relationship in mushy

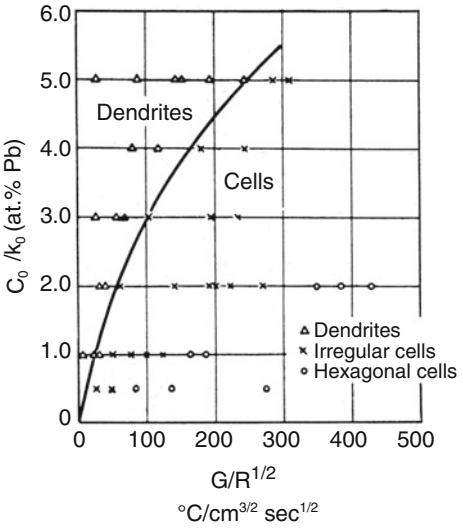

Fig. 4.18 Effect of temperature gradient and growth rate in different composition of Pb on the solidification mode of Sn–Pb alloys [4]

state. However, there is an inverse relationship for temperature and viscosity, (4.23), where higher temperatures impart lower viscosity values. This equation is only valid for systems where there is not any phase change due to temperature variation as, for instance, in polymeric materials.

$$\eta = \eta_o \exp\left(\frac{\Delta E}{RT}\right) \tag{4.23}$$

Where ΔE, η_o, R, and T are the activation energy, initial viscosity, the gas constant, and temperature, respectively.

Holding time (isothermal) is another parameter which affects viscosity due to particle growth. Particle growth in SSM slurries can take place by coalescence, Ostwald ripening, or a combination of both mechanisms. The growth rate of Al–Si alloys in the SSM condition is almost invariably controlled by cube law of the type $R^3 = k_c t$ [74], where the kinetics rate constant is given as (4.24):

$$k_c = \frac{8}{9} \frac{\Gamma D_L}{M_L(C_s - C_l)} f(f_\alpha) \tag{4.24}$$

Where $f(f_\alpha)$ is a function of the solid fraction (its value for globular α-Al particles in A356 is 3.17), Γ is the capillary constant (2×10^{-7} mK), D_L is the solute diffusivity in the liquid (3×10^{-9} m^2 s^{-1}), M_L is the liquidus line slope (6.8 K/at.%Si), C_s is the solute concentration in the solid phase (1.3 at.% Si), and C_l is the solute concentration in the liquid phase [74].

Sample size

Generally the sample size effect on viscosity is not a matter of concern if the homogeneity of temperature and shear rate distribution within the sample is

maintained. Nonetheless it is preferred to perform tests on small size specimens to reduce the cost of testing, since for larger specimens more powerful machines are needed. In addition, smaller specimens may render less diverse results. In rotational viscometry for example, the distance of the annular gap between outer cylinder (cup) and inner cylinder (bob) [7, 32, 33, 51] is always preferred to be as close as possible to make the shear rate distribution more homogenized within the slurry during rotation.

Parallel plate compression viscometry method [75, 76] also uses small size samples. Such matter refers back to mathematical calculation of viscosity for cylindrical samples under parallel plate compression test. Such calculation has been done for Newtonian and non-Newtonian fluid assumption. The mathematical solution is always based on the samples with $h \ll R$ ($h =$ height and $R =$ radius) to reduce mathematical complexity. In fact the term v_z, the velocity along z axis, is neglected against radial velocity, v_r, and the continuity and momentum equations are solved. The effect of sample size was also studied at authors' laboratory using parallel plate viscometry. Lashkari et al. [36, 41] reported that one of the most important aspects of rheological testing is to confirm the irrelevance of sample size effect on the viscosity of SSM billets, at low shear rates, less than 10^{-2} s^{-1}. Two different sets of sample sizes with the aspect ratios of 0.4 (10 mm height 24 mm diameter), similar to those reported in the literature, and 1.8 (140 mm height 75 mm diameter) were prepared and compressed under the same initial pressures, holding temperature, 595 °C, and fraction solid, f_s of 0.33. Based on the assumption of "axial flow is negligible against the radial flow" during quasi-steady-state deformation, it was confirmed that large-scale samples could also be used during parallel plate compression viscometry to study rheological behavior of SSM billets through calculation of viscosity. It was also summarized that the sample size is not the important parameter as given below.

- Morphological evolution due to manipulation of pouring temperature has the greatest effect on the deformation behavior of the SSM A356 alloy where viscosity value decreases from dendritic to globular morphology.
- In the context of sample size, reheating of the thixocast samples may bring about minor morphological and size changes in the primary α-Al particles which could affect the viscosity value. This is particularly true for dendritic morphology while for rosette and globular morphologies the changes in viscosity value due to reheating are negligible.
- The viscosity numbers for the globular morphology prepared at low pouring temperature of 615–630 °C are the same in both rheo-billets (140 mm height 75 mm diameter) and thixo-disks (10 mm height 24 mm diameter) to confirm the irrelevance of $h \ll d$ criterion and the reliability of parallel plate compression test to determine viscosity of SSM slurries.
- The most important parameter to influence the flow characteristics of SSM slurries is the morphology of the primary phase, not the sample size.

4.2.3 Testing Methods

Viscosity is the main parameter to study the rheology of semi-solid metallic alloys. It is an indication of semi-solid metal capability in filling the mold and determines the required force for deformation and material flow. During conventional solidification viscosity rises up steadily with increasing solid fraction till the point where the solid can no longer move freely, dendrite coherency point (DCP), and the already solidified segment tends to develop strength.

In SSM processing, the DCP is postponed due to the forced convection or shallow temperature gradient within the melt through prevention of dendritic network development. The breakdown of dendrites due to stirring coupled with multi directional growth of fragmented dendrites due to more uniform temperature distribution within the mold, i.e., shallow temperature gradient, resulting from forced convection, encourages the formation of equiaxed grains, thus postponing the rapid rise of viscosity to higher fraction of solids as reported by Spencer et al. [7], in their pioneering work on the rheology of Sn15%Pb alloy during early 70s.

There are mainly three experimental routes to characterize the microstructure of SSM billets through analysis of their rheological behavior. They basically relate flow characteristics of SSM billets to its microstructure and viscosity. These are as follows:

1. Fluidity measurement
2. Viscometry
3. Cutting force measurement

4.2.3.1 Fluidity Measurement

For semi-solid metal slurries, the concept of mold filling, fluidity, is a critical issue, since as the concentration of solid fraction increases beyond 0.4–0.5, the viscosity increases so rapidly that makes die filling almost impossible. Furthermore, the behavior of the semi-solid alloy is more complex than one that is fully liquid due to its non-Newtonian nature. Therefore, it is not advisable to use the findings on the fluidity of molten alloys for semisolid metals, although the overall concepts of fluidity may apply for semi-solid metals as well.

The fluidity of molten metals has been widely studied (e.g., [4, 13, 14]) and it is well known that there are the molten metal factor (temperature, viscosity, and latent heat of fusion), the mold–metal interaction (heat flow, thermal conductivity, heat diffusivity, and mold temperature), and finally the test variables (metal head height, channel size, and pouring characteristics including pouring speed) that influence the fluidity. Despite the extensive work carried out on different areas of SSM processing, very few studies have been focused on the fluidity concept [77–83]. It is believed that the solidification mode of semi-solid slurries in a fluidity channel is similar to that of fully liquid alloys and that the slurry flow is stopped by a critical

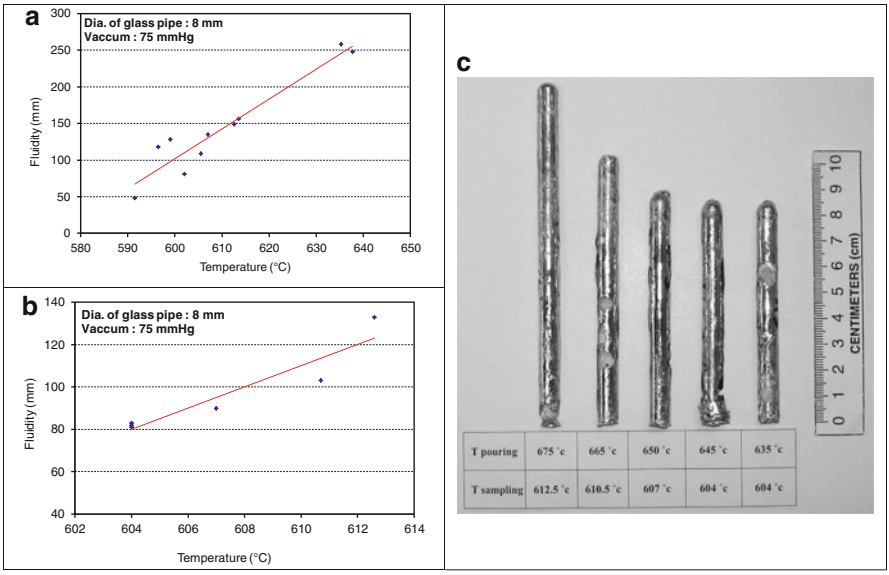

Fig. 4.19 Effect of sampling temperature on the fluidity distance for: (**a**) mechanical stirring, (**b**) SEED process, and (**c**) image of SEED fluidity test results, 356 Al–Si alloy ([78], reprinted with permission of The Minerals, Metals & Materials Society)

solid concentration near the tip of the flow where the solidification is most progressed [79]. Authors studied the fluidity of 356 Al–Si SSM slurries prepared by mechanical stirring and SEED process and showed that the fluidity is directly related to temperature as higher temperatures result in less solid fraction and thus higher fluidity, see Fig. 4.19 [78].

As expected, the distance travelled by the slurry increased with temperature. However, the nature of slurry flow within the glass tube is different for mechanically stirred and SEED processes. For mechanically stirred tests, it appears that as temperature is reduced, the initially formed solid particles acted as filter for the liquid since there is a tendency for agglomeration. Furthermore, the percentage of primary α-Al particles detected within the fluidity samples is only 20 % at its maximum. When compared with the actual solid fraction at temperatures for this alloy, it was clear that more than half of solid particles could not enter the tube used to take slurry sample at the partial pressure of 70 mmHg (used in this study). This was due to agglomeration for mechanically stirred samples and also the increase in particles size with reducing temperature. These particles are then appeared to have acted as filters and thus prevented solid particles entering the tube. Such behavior may suggest that fluidity test of this nature is not a true representative of the slurry characteristics.

4.2.3.2 Viscosity Measurement

Viscometry

There are several test procedures to study the viscoplastic behavior of SSM slurries. These methods are based on measuring the viscosity of slurries and are divided into two main categories depending on the fraction solid, i.e., low fraction solid up to 0.4, and high fraction solid, in excess of 0.4–0.5 [19]. The simplest methods to measure the viscosity of low fraction solid slurries are the direct methods of rotational viscometry where the induced torque in the slurries is measured.

Since the introduction of viscosity concept by Newton, nearly 200 years elapsed before the first practical rotational viscometer was devised by Couette in 1890 [9]. Couette concentric cylinder viscometer consisted of a rotating cup and an inner cylinder which was supported by a torsion wire and rested in a point bearing in the bottom of the cup. This viscometer was a large device with an inner radius, R_{bob}, of 14.39 cm and an outer radius, R_{cup}, of 14.63 cm. Couette design enabled him to calculate the apparent viscosities of non-Newtonian fluids with only a small error because of the very small ratio of gap to inner radius. In Couette-type viscometers, rotation of the cup while holding the bob stationary produces shear stress on the surface of the bob which are measured as torque. Figure 4.20a shows the schematic of the apparatus which was used by several researchers [7, 32, 74]. There is another type of cylindrical viscometers, Searle type viscometer, which is slightly different where the cup is stationary and the bob or inner cylinder rotates and induces shear into the melt or slurry. In both apparatus, the temperature of slurry during stirring process is maintained almost constant by using electric heating elements inside the body of the apparatus. Temperatures are controlled by using thermocouples which are embedded in different sections. Figure 4.20b shows schematic of Searle-type viscometer used by other researchers [23, 33, 51, 61, 62].

Mathematical Treatments

In order to arrive at the fundamental equations for coaxial rotational viscometers, the following assumptions are made [7, 33, 34];

- The liquid is incompressible
- The motion of liquid is laminar
- The streamlines of flow are circles on the horizontal plane perpendicular to the axis of rotation (the velocity is only a function of radius)
- The motion is steady
- There is no relative motion between the surface of the cylinders and the fluid in immediate contact with the cylinders, no slippage
- The motion is two-dimensional
- The system is isothermal

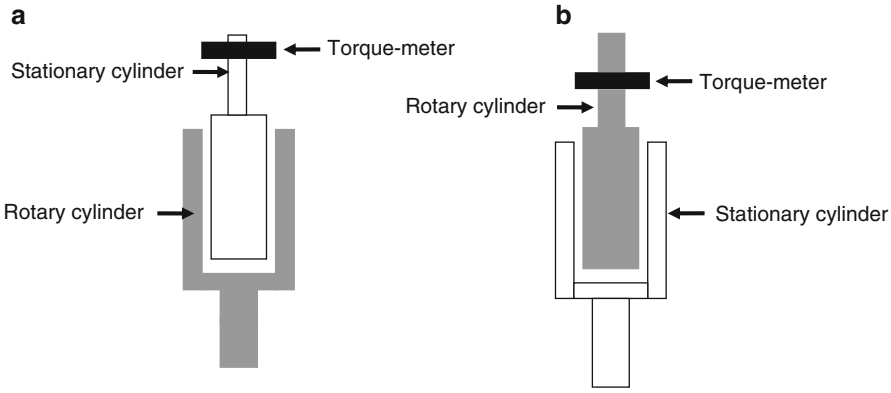

Fig. 4.20 Viscometers; (**a**) Couette type with rotary outer cylinder, (**b**) Searle type with rotary inner cylinder [40]

With such assumptions in both methods the apparent viscosity is calculated by a set of equations (4.25, 4.26 and 4.27) given below using torque data [7, 33, 34].

$$\tau = \frac{T}{2\pi r^2 L} \tag{4.25}$$

$$\dot{\gamma} = \frac{2\Omega}{r^2}\left(\frac{r_i^2 r_o^2}{r_o^2 - r_i^2}\right) \tag{4.26}$$

$$\eta = \frac{T}{4\pi L\Omega}\left(\frac{1}{r_i^2} - \frac{1}{r_o^2}\right) \tag{4.27}$$

Where T is the measured torque, L is the liquid height inside the cylinder, $\dot{\gamma}$ is shear rate, Ω is angular speed of rotor, η is apparent viscosity, r_i is inner cylinder radius, r_o is outer cylinder radius, and r is the actual annular gap radius. There are problems to use coaxial rotating viscometers which are for fluids whose viscosity is related to the geometry of instrument. This is because of the change of shear rate across the gap from the region of higher stress to that of lower stress. Use of the mean rate of shear is permissible only for Newtonian and plastic fluids. Because there is no set relationship between stress and shear rate for pseudoplastic and dilatant fluids, the actual shear rate, presented at (4.26), at any point in the gap cannot be estimated except for extremely small gaps.

Torque measurement is useful to investigate the dendritic coherency point during equiaxed/dendritic solidification. The coherency point is determined as the critical point where the torque increases sharply [48].

Parallel Plate Compression Test

For the high solid fraction slurries, the viscosity is not generally measured by the rotational viscometers. Such self-standing billets (slugs) are more rigid and can only be characterized by other methods including parallel plate compression test [36, 38, 75, 76, 82–89], direct or indirect extrusion [27, 85, 90, 91], indentation test, tensile test [92, 93], and cutting tests [94].

The most common way to examine rheological behavior of paste-like materials is by parallel plate compression test. In this method, a dead weight is simply applied on the top surface of SSM slug and its deformation behavior is investigated by analyzing strain variation versus time [95]. The resulting strain–time graph is further treated mathematically to calculate viscosity and characterize the rheological behavior of tested alloy. The interpretation of results obtained from such graphs can be treated differently depending on the assumption of the SSM slurries behaving as Newtonian or non-Newtonian fluids. In the case of low applied shear rates, less than 0.01 (s^{-1}), the resulting graphs could be treated similar to that of Newtonian fluids [75] with the following equations to calculate the viscosity of the semi-solid cylindrical billets.

The classical Newton's law of viscosity (4.2) was rewritten in terms of the applied force, F (4.28), for a cylindrical sample squeezed between two parallel plates, and with the assumption of the billet not filling the space between the two plates during the course of deformation [21]:

$$F = -\frac{3\eta V^2}{2\pi h^5}\left(\frac{\mathrm{d}h}{\mathrm{d}t}\right) \tag{4.28}$$

Integrating (4.28) for $h = h_0$ at $t = 0$ and $h = h$ at $t = t$, (4.29), and knowing the initial pressure, $P_o = \frac{Fh_o}{V}$, at the onset of deformation, the viscosity–time relationship is given in (4.30):

$$\frac{1}{h^4} - \frac{1}{h_o^4} = \frac{8\pi F t}{3\eta V^2} \tag{4.29}$$

$$\frac{3Vh_o}{8\pi P_o}\left(\frac{1}{h^4} - \frac{1}{h_o^4}\right) = \frac{t}{\eta} \tag{4.30}$$

The viscosity is calculated as the inverse slope of a graph where the left-hand side of (4.30), $\left[\left(\frac{3Vh_\circ}{8\pi P_\circ}\right)\left(\frac{1}{h^4} - \frac{1}{h_\circ^4}\right)\right]$, is plotted against time, (t). For Newtonian fluids, the average shear rate, $\dot{\gamma}_{\mathrm{av}}$, at any instant during compression test is calculated as (4.31) [21]:

$$\dot{\gamma}_{av} = -\sqrt{\frac{V}{\pi}}\left(\frac{\mathrm{d}h/\mathrm{d}t}{2h^{2.5}}\right) \tag{4.31}$$

where v_x, η, V, h_o, h, F, and t are deformation speed (ms^{-1}), viscosity (Pa-s), volume of specimen (mm^3), initial height (mm), instantaneous height (mm), applied dead weight (N), and deformation time (s), respectively. The mathematical solutions employed to reach the above-mentioned equations, (4.28)–(4.31), could be found in Appendix A [38].

If the SSM billets are treated as non-Newtonian fluids, the solution to the flow equations for cylindrical sample squeezed between two parallel plates is as follows (see Appendix A):

$$\frac{h_o}{h} = \left\{1 + \left(\frac{3n+5}{2n}\right) k h_o^{\frac{n+1}{n}} t\right\}^{\frac{2n}{3n+5}} \tag{4.32}$$

where

$$k = \left\{\left(\frac{2n}{2n+1}\right)^n \left(\frac{4(n+3)}{\pi m d_o^{n+3}}\right) F\right\}^{\frac{1}{n}} \tag{4.33}$$

Equation (4.32) is only valid for deformation under steady-state condition where the engineering strain changes linearly with time. (4.32) could be further treated mathematically [38] to include engineering strain (e) as given in (4.34).

$$\log(1-e) = -\left(\frac{2n}{3n+5}\right)\log t - \left(\frac{2n}{3n+5}\right)\log\left(\frac{3n+5}{2n} k h_o^{\frac{n+1}{n}}\right) \tag{4.34}$$

In order to calculate the values of m and n, the logarithmic of engineering strain, log ($1-e$), should be plotted against time, log t, and the slope of such graph and its intercept with strain axis should provide the necessary means to calculate m and n [21]. Figure 4.21 shows schematically a parallel plate compression test machine and the actual in-house designed and fabricated of a large-scale parallel plate compression machine to characterize the microstructural evolution of SSM prepared billets (slugs) [95].

For rheological tests, the as-poured billets were transferred (at temperature 598 ± 2 °C) and compressed uniaxially in the parallel plate compression test machine by applying 2.2 kg dead weight at 598 ± 2 °C. The applied force and resulting displacement were monitored using a load cell with 0.02 % precision and a displacement transducer with ±(0.1–0.2)% full stroke precision. A cylindrical furnace was installed on the press bed to keep the billet temperature constant during the compression tests. The furnace was equipped with quartz heat-resistant windows to allow one to view the billet. Two K-type thermocouples were positioned within the furnace to control the chamber temperature with a precision of ±2 °C. All samples were taken out of the furnace after 10 min of compression and quenched in water to room temperature.

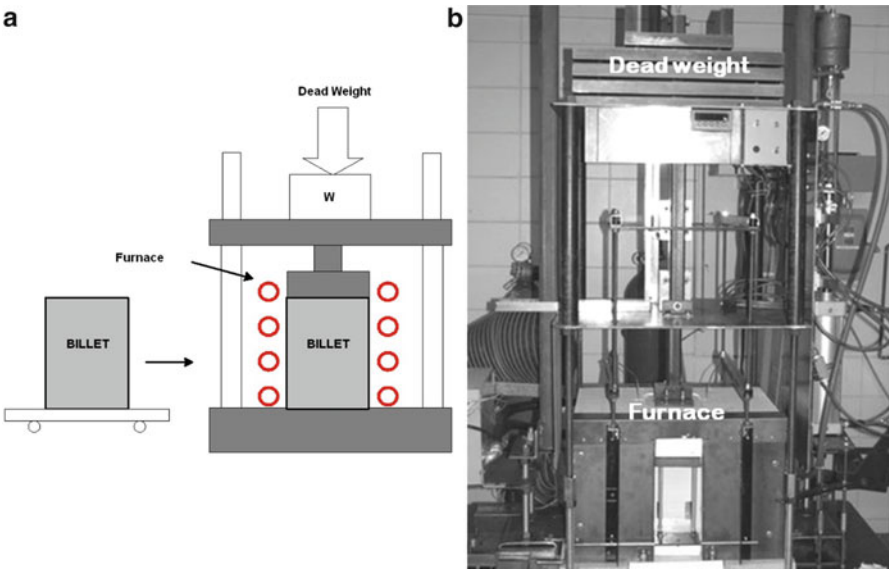

Fig. 4.21 Schematic (**a**) and a real overview of the press (**b**) [95]

Drop Forge Viscometry

Drop Forge Viscometer is a special case [84, 86] of parallel plate compression test where similar equations are used to calculate the viscosity. Such instrument is designed to provide a wide range of shear rates for viscometry tests, 10^{-5} to 10^{4} (s^{-1}). Usually the high shear rate tests is performed within thousandth of second and can just investigate the transient part of the viscosity for thixotropic SSM materials. The developed equation used in such manner is given in (4.35) as a modification of (4.28):

$$m_p\left(\frac{\mathrm{d}^2h}{\mathrm{d}t^2}+g\right)=\frac{-3\eta V^2}{2\pi h^5}\left(\frac{\mathrm{d}h}{\mathrm{d}t}\right) \tag{4.35}$$

Where m_p is the mass of upper plate and g is gravitational acceleration. After calculating the derivatives and knowing the variables in (4.35), the viscosity can be calculated as a function of time.

Sherwood et al. [96, 97] have also developed mathematical equations to calculate viscosity of non-Newtonian materials squeezed plastically between two parallel plates, where the squeezed material fills the space between two platens. Assuming "σ_f" as the friction stress in plate/work piece interface and "σ_y" as the yield stress of the material, the following equation (4.36) is presented to specify the deformation behavior of the substance during compression viscometry.

$$F = \frac{2\sigma_f \sigma_y \pi r^3}{3h_o} + \frac{\sqrt{3}\sigma_y \pi r^2}{2}\left[\sqrt{\left(1-\sigma_f{}^2\right)} + \frac{1}{\sigma_f}\sin^{-1}\sigma_f\right] \tag{4.36}$$

where F is total force required to compress the material, h_o is initial height, and r is the radius of circular platens, where the squeezed material fills the space between them. The force, F, is independent of the compression rate, $\left(\frac{dh}{dt}\right)$, as should be expected from an analysis based upon rate-independent plasticity theory. Kolenda et al. [83] have also used similar equation as (4.36) for evaluating the viscosity of two types of ceramic powders blended together as a ceramic paste. The resulted data indicated the ceramic paste behaving as non-Newtonian materials.

Direct and Indirect Extrusion

Extrusion tests may also be used to study the ability of the SSM billets to fill die cavity by providing information on the viscosity of semi-solid material. Figure 4.22 illustrates extrusion tests schematically along with related graphs [90, 93]. More experimental details and suitable theoretical treatments, mathematical equations, for such methods are accessible in the literature [74, 90, 93, 98].

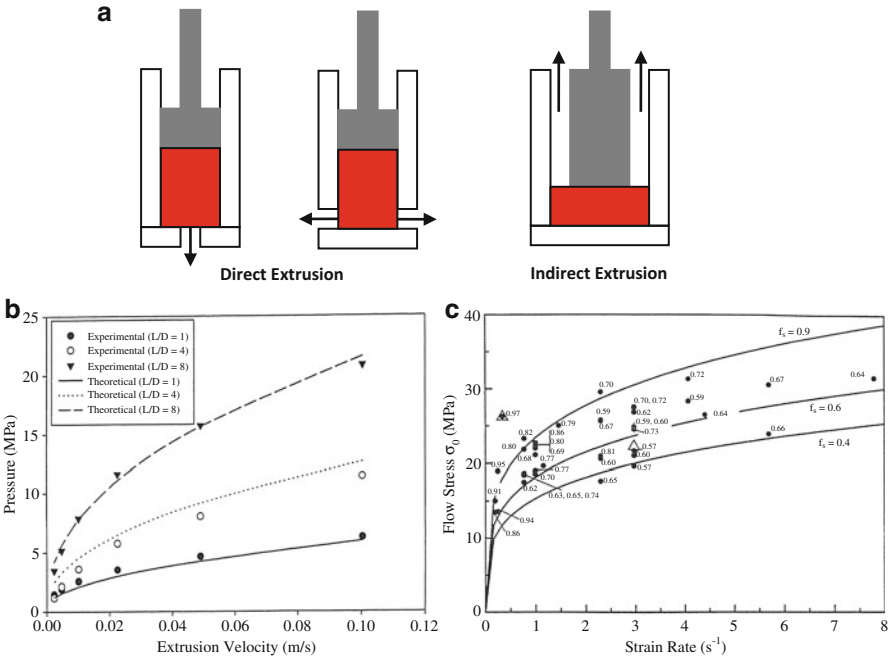

Fig. 4.22 (**a**) Different ways of extrusion viscometry, (**b**) Pressure versus Extrusion velocity graph, comparison of theory and experiments at different dimensions [90], (**c**) Flow stress versus strain rate graph at different fraction solid [91]

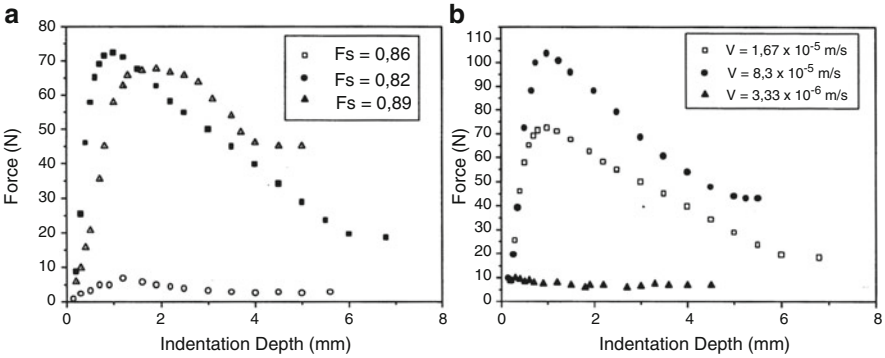

Fig. 4.23 Results of the indentation test for (**a**) constant penetration speeds and different fractions solid (**b**) different penetration speeds and constant 0.86 fraction solid [92]

Indentation Test

Indentation test is another simple way to study mechanical properties of SSM slugs. In this method, the depth of penetration of a steel cylinder under a constant pressure in the semi-solid billet is taken as an indication of viscosity of the alloy. This is a simple test and can be commercialized for online testing of SSM billets. Figure 4.23 shows the effect of testing parameter and fraction solid on the indenter/SSM billets interaction [92]. The following equation (4.37) was used to calculate the viscosity of SSM specimens during indentation test:

$$\eta = \frac{16\pi[(1-\upsilon^2)F]}{6r\dot{\varepsilon}} \tag{4.37}$$

where υ is Poisson ratio, F is the applied load, r is the radius of cylindrical indenter, and $\dot{\varepsilon}$ is the strain rate. It has been shown the pseudoplasticity behavior of Al–4%Cu alloy around 0.82–0.85 fractions solid and solid-like behavior for fractions in excess of 0.85 [92].

Some researchers have also applied the tensile test method for rheological study of semisolid materials [92]. However, both of tensile and indentation tests are not suitable for fraction solid less than about 0.85 [16, 92]. The indentation test is similar to compression tests with more constraints.

Lahaie et al. [99] proposed a physical model to show the relationship between tensile strength and semi-solid parameters, (4.38):

$$\sigma = \frac{\eta\dot{\varepsilon}}{9}\left(\frac{f_s^m}{1-f_s^m}\right)^3\left[\left(1-1/2\left(\frac{f_s^m}{1-f_s^m}\right)\varepsilon\right)^{-3}+2\left(1+\left(\frac{f_s^m}{1-f_s^m}\right)\varepsilon\right)^{-3}\right] \tag{4.38}$$

Thus, from (4.38), the mechanical response, i.e., tensile strength (σ), of the semi-solid body is dependent on the viscosity of intergranular liquid, η, the applied strain

rate, $\dot{\varepsilon}$, the accumulated strain, ε, the solid fraction, f_s and a microstructural parameter, m, bounded by the values 1/2 and 1/3, corresponding to columnar and equiaxed microstructure, respectively. A similar equation has also been used by Wahlen [27] during compressive rheological test of aluminum alloys.

4.2.3.3 Cutting Force Measurement

The apparatus is basically designed as a quality control tool in production line. In this method, semi-solid slurry is cut by a steel blade or wire. The machine has a load cell to measure the force and sensors to determine the speed as well as the wire/blade tension. The speed of cutter to pass through the SSM billet and the resistance of slurry against the passage of cutting blade, the force to be exerted on the blade, is an indication of microstructural feature [52, 94]. Figure 4.24a shows the apparatus during a test. Figure 4.24b describes four indicators used to characterize the cutting curve:

(a) The maximum force
(b) The peak distance
(c) The area under the curve for the first half diameter of the slug corresponding to the cutting energy
(d) The central force relating to the average cutting force at the center of the slug (between 30 and 40 mm)

An example of the results is presented in Fig. 4.25a for three pouring temperatures of 675, 655, and 635 °C for A357 aluminum alloy (test performed at 590 °C billet temperature). A higher pouring temperature results in more dendritic microstructure which is expected to put more resistance against the blade to cut through the billets than globular microstructure. The average value for all four indicators increase with the pouring temperature and one example is presented in Fig. 4.25b.

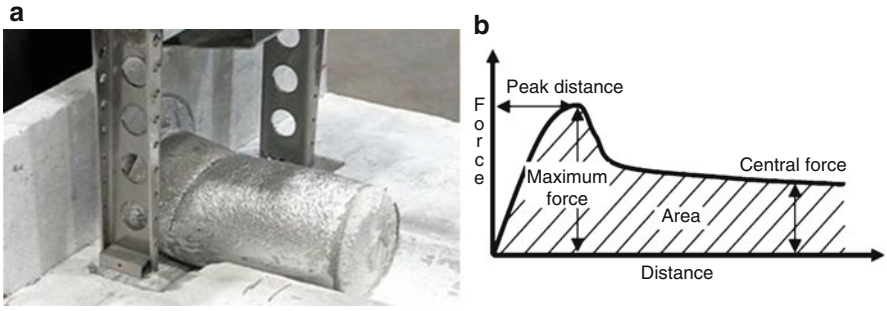

Fig. 4.24 (**a**) Cutting test, (**b**) schematic of a typical Force-cutting distance with four indicators [52]

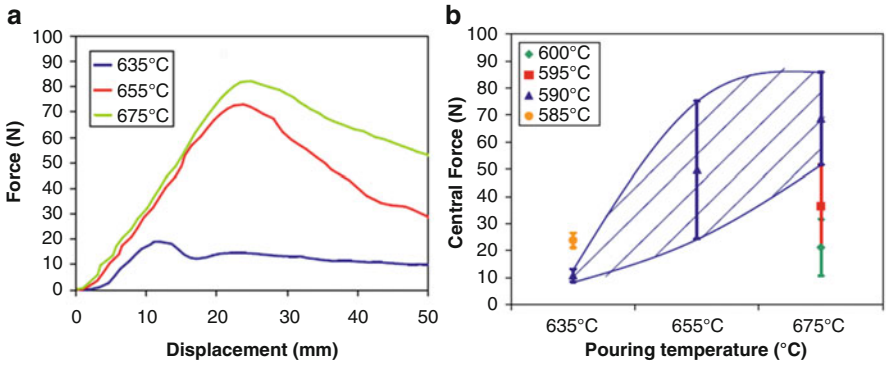

Fig. 4.25 (**a**) Force-displacement curves obtained at various pouring temperatures, (**b**) maximum force - pouring temp for different cutting temperatures [52]

4.3 Micro/Macro Structural Analysis

In addition to thermal characterization of the solidification process during SSM processing and rheological analysis of the as-cast SSM billets, the quality of semifinished SSM billets or the finished SSM products may be studied by macro and microstructural analysis of the constituent phases.

In order to generate a semi-solid structure, the alloy system plays the key role where the coexistence of liquid and solid within a temperature range is the prerequisite for the slurry preparation. The mechanics and mechanisms of the primary particles' evolution, dendrite-to-equiaxed transformation, is the next concern since the formation of globular morphology is expected to enhance die filling and improve mechanical properties of as-cast parts. The ideal microstructure for SSM slurry is fine, spherical solid particles uniformly distributed within a liquid matrix. The solid fraction should be considered carefully, since low fraction solid may lead to handling and mold filling difficulties due to insufficient viscosity and turbulence while high fraction solid may have die filling troubles or increase the cost of machinery.

Based on the aforesaid requirements, characterization of semi-solid material is a necessity to confirm, modify, and obtain an optimum structure for SSM component shaping process. This knowledge not only provides an idea about the material, but also leads to better understanding of rheological behavior and eventually improve the mechanical properties of cast pieces. This is the main theme of this section where qualitative and quantitative metallography principles are implemented to further characterize SSM billets and products [100].

4.3.1 Qualitative Metallography

In order to be able to accurately characterize SSM microstructure, it is necessary to understand the features and complexity of the resulting solidified structures and be able to differentiate between the observed two-dimensional (2D) structure and the actual three-dimensional (3D) morphology.

Normally after initial visual inspection, the microstructure of the solidified alloy is observed on the plane of polished surface using optical microscopy. The 2D analysis may not present a complete picture of the structure and sometimes could lead to invalid conclusions. This is particularly true for cases where in spite of a well distributed primary phase in 2D plane, the interconnectivity of isolated primary particles from underneath the plane of polish has resulted in misleading conclusions on the process efficiency.

In literature, there are different techniques employed to reveal the true morphological evolution of primary phase including reconstruction of 3D images by serial sectioning, X-ray micro-tomography, and finding the crystallographic orientation relationships by electron backscatter diffraction pattern (EBSD).[3] Serial sectioning is a destructive technique based on the successive grinding and polishing of the sample with capturing the consequent images. The major difficulties are calibration of the sectioning distance and also the working frame. These shortcomings are overcome by automatic polishing procedure and drilling guides and controlling holes perpendicular to the polished section. The morphology of primary particles together with their possible interconnectivity is characterized based on the position and shape of each feature along these serial sections. The final 3D image is constructed with the support of computer software [103–107]. An example is presented in Fig. 4.26.

For 3D visualization, X-ray microtomography was developed by Suery and his coworkers at Grenoble, France. The nondestructive technique is based on the X-ray beam passing across the sample with consequent capturing the transmitted image by a CCD or CMOS camera. The specimen is placed on a high precision rotating table in the trajectory of an X-ray beam. Part of the X-rays is absorbed whereas the transmitted X-rays are converted into visible light using a scintillator. The sample is then rotated over 180° or 360° and during this rotation, sufficient projections are recorded. The final stage is the same as serial sectioning method which is retrieving

[3]Electron Backscatter Diffraction "EBSD" is a technique which provides crystallographic information by analyzing crystalline samples in the scanning electron microscope "SEM." In EBSD, a stationary electron beam strikes a 70° tilted sample and the diffracted electrons form a pattern on a fluorescent screen. This pattern is unique to the crystal structure and orientation of the sample region from which it was generated. The diffraction pattern is used to measure the crystal orientation, grain boundary misorientations, discriminate between different materials, and provide useful information about local crystalline perfection. By scanning in a grid across a polycrystalline sample and measuring the crystal orientation at each point, the resulted map will reveal the constituent grain morphology, orientations, and boundaries. In addition, the data shows the preferred crystal orientations (texture) present in the material [101, 102].

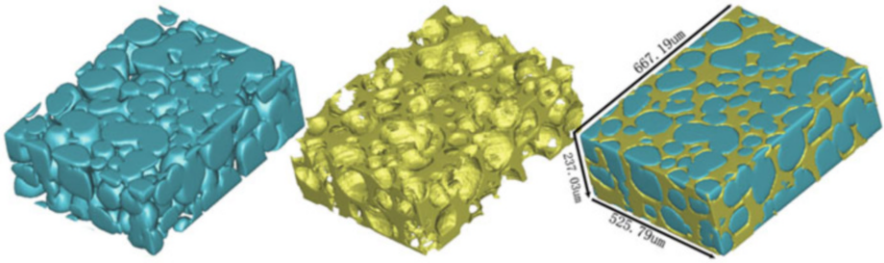

Fig. 4.26 Three dimensional morphology of A356 slurry reconstructed by serial sectioning of 60 consecutive images (Courtesy of Prof. Xiangjie Yang) [107]

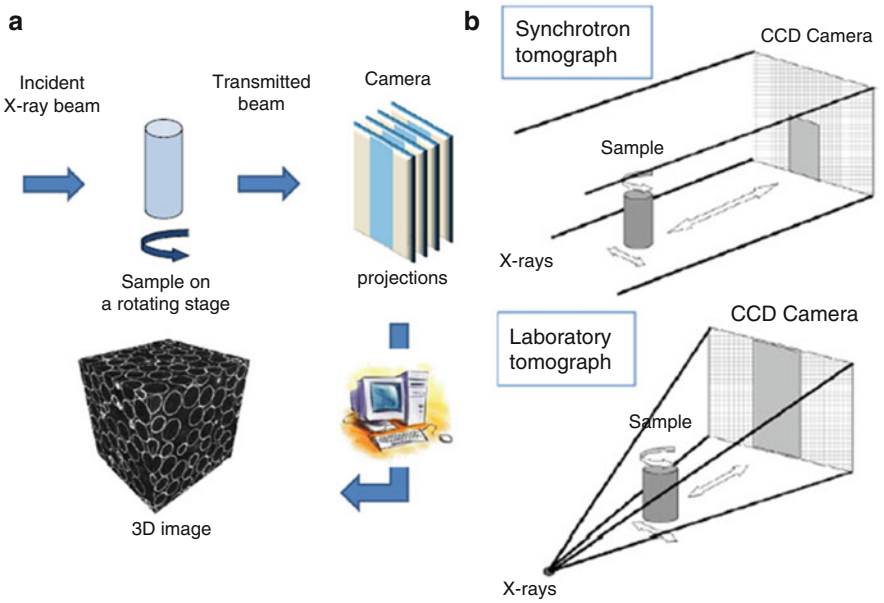

Fig. 4.27 (**a**) Principle of tomography, (**b**) synchrotron and laboratory tomography [108]

a 3D image of the sample [108]. In this method, the contrast between the phases is directly related to the atomic number difference between various phases and the fact that solid and liquid have good absorption contrast due to the large difference in chemical compositions. Previously, the technique was used at room temperature however by the development of the technique, in situ scanning in the semisolid state is viable [108–110].

According to Salvo et al. [108], tomographs are classified into two categories (Fig. 4.27): laboratory tomographs with divergent X-ray beam and polychromatic and the synchrotron sources (ESRF, SOLEIL in France, SLS in Switzerland, Spring 8 in Japan, etc.) where the X-ray beam is parallel, polychromatic, or monochromatic.

Kareh et al. [109] used synchrotron X-ray tomography to study the deformability of Al15Cu during indirect extrusion process in a small scale. The specimen

originally heated to ~5 °C above the eutectic temperature for 200 h. A specimen from original material then heated to 10 °C above the eutectic temperature at around 558 °C to form 0.73 solid fraction. It was then held for 5 min before isothermal indirect extrusion at a ram speed of 0.01 mm s^{-1}. Figure 4.28 presents

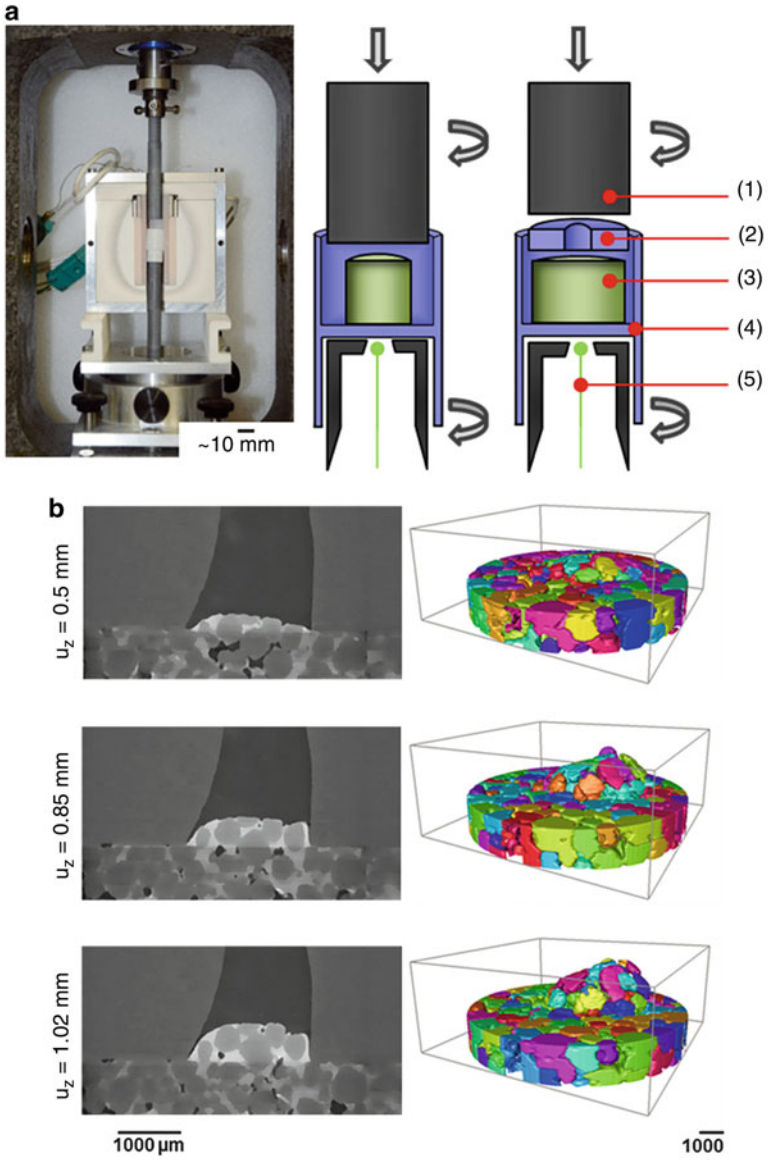

Fig. 4.28 (**a**) Experimental setup showing the actual machine and schematic of the compression setup "(1) ram, (2) boron nitride extrusion die, (3) specimen, (4) container, (5) thermocouple" (**b**) microstructure at three instances during semisolid extrusion (*left* is "xz" slices, *right* is 3D rendering of the solid) (α-Al gray, Cu-enriched liquid white, and pores dark) [109]

three snapshots in time showing filling process as well as a 3D rendering of the separated α-Al globules extruding upward only.

A modern technique is based on the automated serial sectioning using Focused Ion Beam (FIB) and generating crystallographic information with electron backscatter diffraction (EBSD) which is installed in a combined FIB-SEM instrument. The process of FIB slicing and EBSD mapping is repeated several times before assembling the individual 2D information together into a 3D viewer. By using this technique, it is possible to Ion-beam mill a series of slices followed by mapping them by EBSD and using computing software for 3D crystallographic maps. This allows the quantification of the spatial distribution of various crystallographic features of the microstructure [111, 112].

The current section is mainly concerned with microstructural characterization of the SSM cast parts where certain complexities may generate misleading results. With the polarized light microscopy[4] [113] and image analysis, it is tried to differentiate SSM microstructural features to render more reliable characterization (in addition to microscopy-based routes, there are rheological tests, as production-line quality checks, to differentiate between globular and dendritic structures which was elaborated comprehensively before).

4.3.1.1 Dendritic and Nondendritic Distinction

Occasionally and depending on the process parameters, solidification conditions may lead to dendritic growth in all or portions of the semi-solid billet, as for example the most prone area for dendritic solidification is near the mold wall. As a result, the final polished microstructure may show dendrites' main trunks and their branches. Also in some segments, isolated individual globules could be observed which are not real globules. Hence, the way dendrites intersect the polished surface may generate numbers of pseudo individual and isolated particles (Fig. 4.29).

The conventional bright field and polarized light micrographs in Fig. 4.30 confirm the deficient nature of analysis carried out on 2D sections. The dendrite secondary branches are treated as individual and isolated particles if processed by an image analyzing system. This leads to erroneous calculation of parameters attributed to particle size and morphology such as average circular diameter and sphericity where a dendritic structure is wrongfully interpreted as globules.

[4]Metallographic etching is defined as the procedure required to be implemented to expose particular microstructural features of interest which normally are not evident in the as-polished condition. Anodic oxidation "anodizing" is an electrolytic etching depositing an oxide film on the surface and developing grain coloration that is detectable by cross polarized light. It was noted that in certain nonferrous alloys that have noncubic crystallographic structures such as magnesium, titanium, and zirconium, grain size can be identified efficiently in the polished condition while this is not possible for metals with cubic, isotropic crystal structure (using polarized light). Anodized surface films on cubic metals, such as aluminum, are usually examined under polarized light to reveal grain contrast [113].

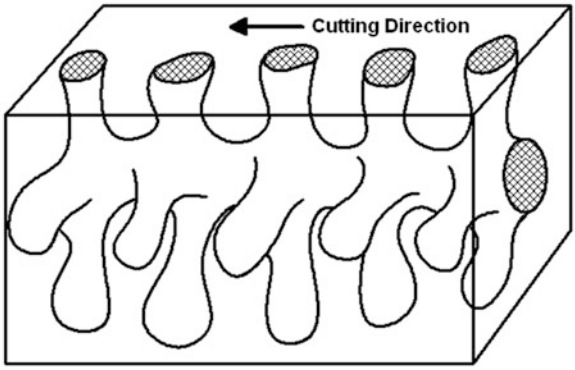

Fig. 4.29 3D view of dendrite-polished surface intersection (reprinted with permission of The Minerals, Metals and Materials Society) [100]

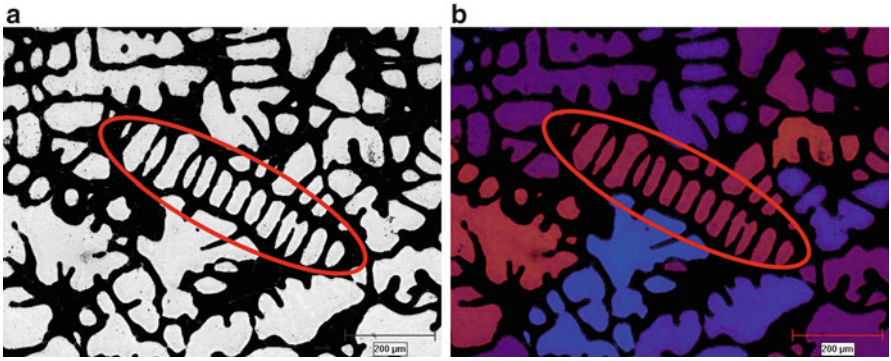

Fig. 4.30 Branches of dendrite with: (**a**) bright field, and (**b**) with polarized light, A356 alloy, quenched from 598 °C

Another case to explore the difference between dendritic and globular morphologies is using electron backscatter diffraction (EBSD) analysis as shown in Fig. 4.31. These grain maps belong to two different pouring temperatures (690 and 625 °C) for 356 commercial Al–7%Si alloy (melting temperature is around 615 °C). In EBSD, grains have different interpretation from that of the traditional metallography. In this method, two neighboring scan points belong to the same grain if the crystallographic misorientation between them is less than a defined value (normally 10 or 15°) [101, 102].

4.3.1.2 Pseudo-Globule

Primary particles in semi-solid microstructure have complex morphology. For instance, the particle that is supposed to be one globule may be interconnected to other globules and thus the proper nomenclature for such particle is "pseudo-

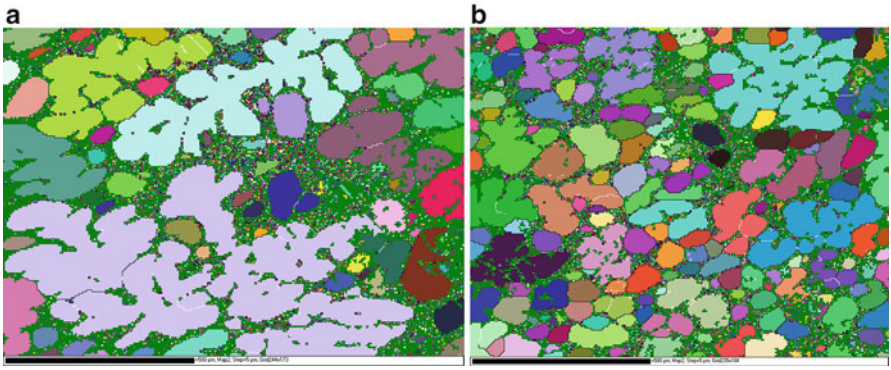

Fig. 4.31 Grain mapping of two different pouring temperatures for 356 commercial Al–7%Si alloy, (**a**) 690 °C, and (**b**) 625 °C (melting temperature is around 615 °C) (each grain is assigned a color to distinguish them from other neighboring grains) (black scale bar is 500 μm)

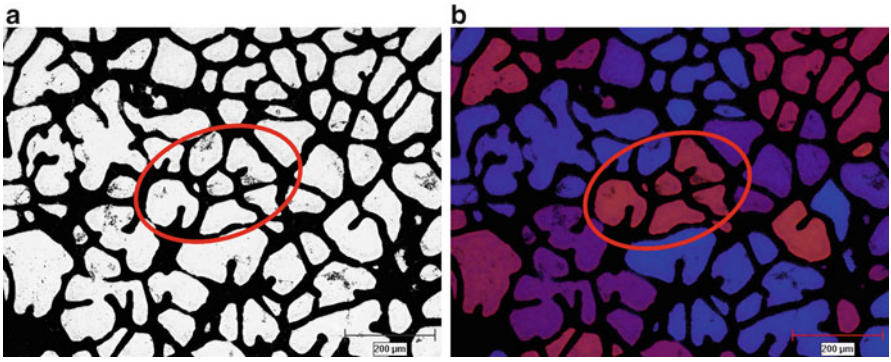

Fig. 4.32 Formation of cramped dendrite: (**a**) bright field illumination, (**b**) polarized light, A356 alloy quenched at 598 °C

globule." The concept of pseudo-globule could be easily understood by comparing different particles seen in the optical micrograph of Fig. 4.32. The typical encircled globules appear to be isolated. However, polarized light microscopy distinctly reveals the isolated particles have identical color contrast, and therefore originated from one particle.

This phenomenon is more prevalent in stir-based processes such as mechanical or electromagnetic stirring routes. By stirring, the resulting forced flow obliges the preformed dendrites to break up by mechanical fragmentation [4] or dendrite root remelting mechanisms [114]. However, if the applied shear force is not sufficient enough to disintegrate the branches, they may plastically bend to form the so-called cramped dendrites. Therefore, it is expected to have different colors for the isolated particles in the former case, true isolated particles, while similar color contrast should be expected in the latter case, cramped particle. The pseudo-globules seen in

Fig. 4.32 may have their origin in the cramped dendrites. These particles are not the result of agglomeration of isolated spherical particles since they have the same color contrast and therefore an interpretation based on the bending and intertwining of dendrites could be a valid conclusion. The only justification for such isolated particles is due to the metallographic 2D sectioning. Pseudo-globules have a key role on the rheological properties of SSM slurries and results in higher viscosity.

Breaking and fragmentation of primary dendrites by mechanical stirring is the original route for SSM processing. However in such structures, there are large primary agglomerations which have very complex shape. These groups of primary particles seem to have formed due to agglomeration of small and individual particles which is not an accurate assumption. Investigation on agglomerated particles goes back to the work of Ito et al. [106] on particles formed during mechanical stirring of Al–6.5%Si. The prepared SSM slurry was sheared at a rate of 900 s^{-1} for 2 h at 0.2 fraction solid and then quenched. The quenched sample was polished and examined in successive sections of 10–20 μm apart. By reconstruction of the 3D model from such serial sections, particles which appear to be isolated are actually interconnected to others. Figure 4.33 is a 3D reconstruction of this microstructure showing the bulk of the particles in the region studied are interconnected to form single agglomerate.

The idea was verified [58] by finding the crystallographic orientation relationship between agglomerate particles in Al–6.5%Si using electron backscatter diffraction technique, EBSD. In the same study, it has been stated that all particles belonging to the same agglomerate are related either by low angle grain boundaries

Fig. 4.33 3D reconstruction showing the interconnection of single agglomerate (reprinted with permission of The Minerals, Metals and Materials Society) [106]

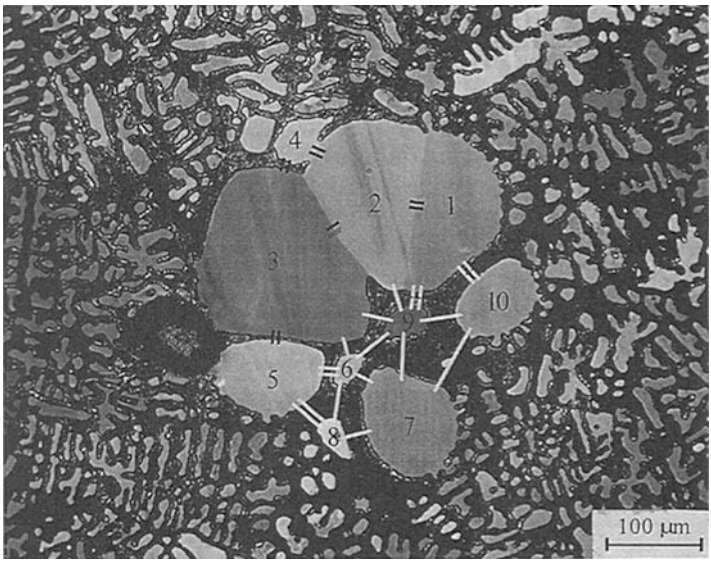

Fig. 4.34 Agglomerate of ten particles. The bonds marked (–) indicate a low angle grain boundary (0–10°), while bonds marked (=) indicate a misorientations of $60 \pm 5°$ with the rotation axis close to the [111] axis (reprinted with permission of The Minerals, Metals and Materials Society) [58]

with misorientations less than 10° or by misorientations about 60° around the [111] axis which corresponds to coherent twins. Figure 4.34 and Table 4.3 show an agglomerate of ten particles in which all particles have at least one neighboring particle with one of the two observed orientation relationship. As for instance, particle number 9 has an orientation relationship to particles 2, 3, 6, 7, and 10 corresponding to a low angle grain boundary, while it has an orientation relationship to particle 1 corresponding to a coherent twin boundary. This confirms that particle 9 is connected to the rest of the particles associated to the agglomerate through the third dimension [58].

In another study, Niroumand et al. [103] used Al–10.25%Cu and mechanical stirrer and by serial sectioning proved that the microstructure of slurry consists of pseudo-particles / clusters in polished surface. Many researchers have interpreted this phenomenon as a process of agglomeration of small globule particles and identified them as single primary grains, but in reality, the majority of these particles were interconnected from underneath (3D) three dimensionally. Figure 4.35 shows a pseudo-cluster and resulting 3D model of the sample indicating the structural complexity.

As described earlier, X-ray microtomography is a real-time tool which is quite capable of constructing the development of SSM structure during solidification process. In fact by analyzing the high resolution image, it is possible to visualize the solid phase formation procedure and see if the primaries are isolated or interconnected. Figure 4.36a shows a 3D view of A356 alloy isothermally held at 587 °C for 10 min. By removing the liquid from 3D image, the connection among solid particles become obvious, Fig. 4.36b [16].

Table 4.3 Misorientations data between particles in the agglomerate shown in Fig. 4.34 (relative misorientations θ, the rotation axis [h, k, l], and the deviation $\Delta\varphi$) (reprinted with permission of The Minerals, Metals and Materials Society) [58]

Particles	θ	[h, k, l]	$\Delta\phi$	Interface type
1–2	59.6	[1,1,1]	0.9	Coherent twin
2–3	3.7	[1,3,6]	2.8	Low angle
2–4	56.3	[1,1,1]	5.2	Coherent twin
3–4	55.8	[1,1,1]	8.8	Coherent twin
3–5	56.8	[1,1,1]	13.6	Coherent twin
3–6	3.4	[1,4,5]	12.4	Low angle
5–6	57.2	[1,1,1]	12.4	Coherent twin
5–8	55.6	[1,1,1]	7.9	Coherent twin
6–8	10.3	[0,2,3]	2.3	Low angle
6–7	4.1	[1,1,3]	2.5	Low angle
7–8	6.9	[1,3,3]	2.5	Low angle
7–10	6.7	[1,2,3]	8.4	Low angle
10–1	56.1	[1,1,1]	7.8	Coherent twin
9–1	59.1	[1,1,1]	3.3	Coherent twin
9–2	2.8	[2,3,3]	1.6	Low angle
9–3	6.4	[1,2,3]	0.7	Low angle
9–6	5.9	[1,6,8]	0.3	Low angle
9–7	4.9	[1,2,10]	2.1	Low angle
9–10	7.3	[2,3,6]	1.6	Low angle

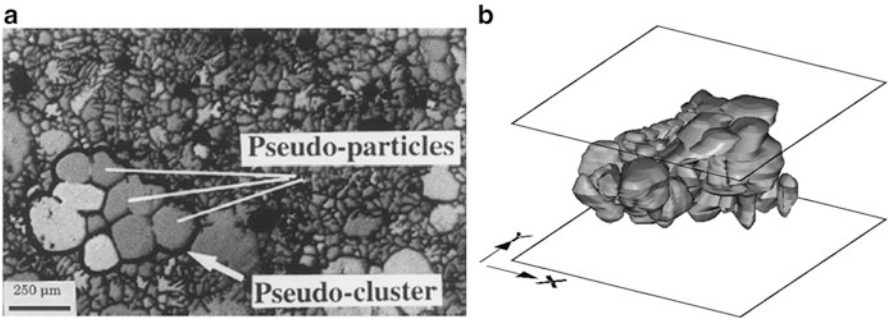

Fig. 4.35 (**a**) Definition of pseudo-particles and pseudo-clusters, (**b**) CAD generated view of a 3D rendered pseudo-cluster [103]

4.3.1.3 Sintering and Coalescence

Sintering and coalescence of primary particles are the other mechanisms active during SSM processes. It is envisaged during stirring the solid particles collide with each other to form welded joints which are eventually strengthened due to high temperature and easy diffusion.

Observation of unusual grain boundaries goes back to the work of Apaydin et al. [114] on the Al–10%Mg which was stirred with different stirring periods and shear rates at low cooling rate (1.5 K min^{-1}) (Fig. 4.37). It was claimed that these

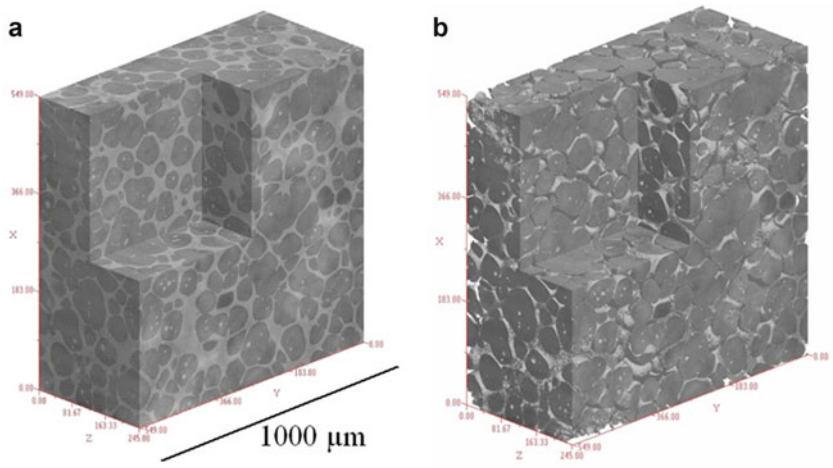

Fig. 4.36 3D image of A356 alloy isothermally held at 587 °C; (**a**) solid and liquid phases, (**b**) only solid phase [16]

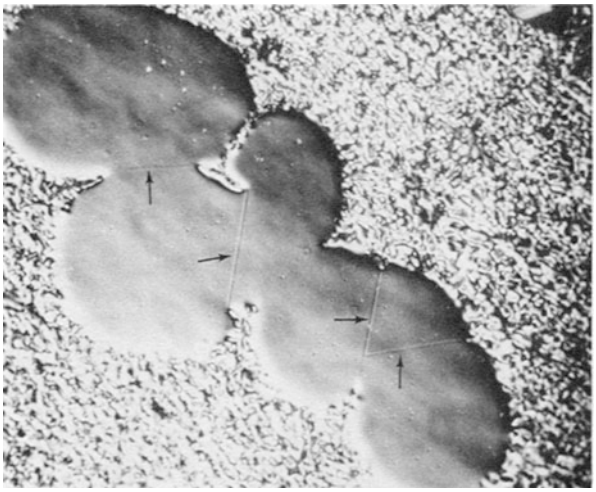

Fig. 4.37 Optical micrograph of a particle showing four special boundaries in Al–10%Mg alloy stirred 7 min at 400 s^{-1}, ~×193 [114]

special boundaries are low energy boundaries since they did not show precipitation during solution and aging treatments. They postulated that these special boundaries are probably produced by sintering where the initial particle–particle contact resulted from particles collision due to stirring. The other possibility for special boundary formation is the growth twining mechanism. Generally in aluminum and its alloys, the (100) facets preferentially grow in the direction opposite to the heat flow [4]. However, if this growth preference is disturbed in any manner (such as by introduction of solute elements or by agitation), more of the (112) facets grow in

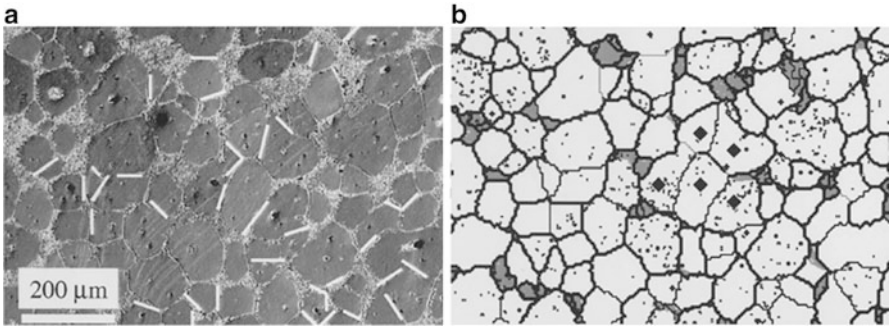

Fig. 4.38 Grain structure in EM stirred and grain refined Al-6082, poured at 700 °C, (**a**) secondary electron image, all special boundaries are marked with *white lines*, (**b**) grain boundary map. Low-angle and coherent twin boundaries are indicated with thin lines [60]

direction opposite to the heat flow and resulting in a nucleation for growth twining on the solid–liquid interface [114].

Figure 4.38a is a secondary electron image of an electromagnetically stirred "EMS" sample of Al-6082 alloy, isothermally held at 638 °C for 10 min [60]. By EBSD investigation, all special grain boundaries were characterized and shown by white lines in Fig. 4.38a. Figure 4.38b is a grain boundary map of the same area (the white grains represent unmelted material and the gray regions are quenched melt). High angle grain boundaries are marked with thick black lines whereas low-angle and twin boundaries are marked with thin lines. The diamonds highlight six grains separated by low angle and twin boundaries and accordingly belong to the same agglomerate. It was claimed that formation of a normal grain boundary would be energetically unfavorable as some solid–liquid interface with energy of 95 mJ m^{-2} would be replaced by a grain boundary with energy of 324 mJ m^{-2} [60]. Low angle grain boundaries and coherent twin boundaries, on the other hand, would form readily since they have lower interfacial energy than the solid–liquid interface having high angle boundaries.

An example of sintering in SSM materials is shown in Figs. 4.39 and 4.40. Two or more isolated solid particles joined and formed a pseudo cluster which is associated, for instance, to the stabilized contact during the stirring (arrows show solid necks). This effect could be seen in regions with low stirring or stagnant liquid and solid. Different globules present different primary α-Al particles with various orientations. Thus, sintering of individual primary particles could be easily detected by different color contrasts by color metallography or EBSD technique. In the semi-solid science, this is defined as "agglomeration" [17–19] where primary particles, basically consisted of simple isolated globular or rosette shape, come into contact and sinter together to form agglomeration. Particles become interconnected by solid necks and further spheroidized by material transport specifically through the neck area which has a negative curvature. The sintering mechanism has been assumed to occur under condition $\gamma_{gb} < 2\gamma_{sl}$ in which γ_{gb} and γ_{sl} are grain boundary and solid–liquid phase boundary energies, respectively. As mentioned by Doherty et al. [115],

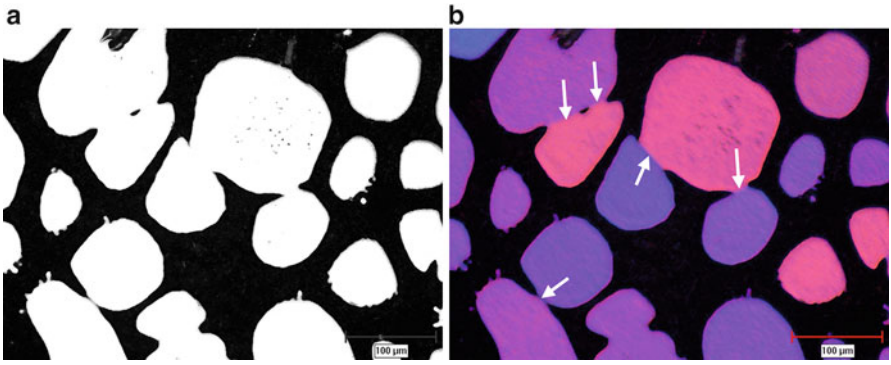

Fig. 4.39 Sintering effect of globules with bright field (**a**) and polarized light application (**b**), Electromagnetically Stirred A356 alloy, reheated at 593 °C

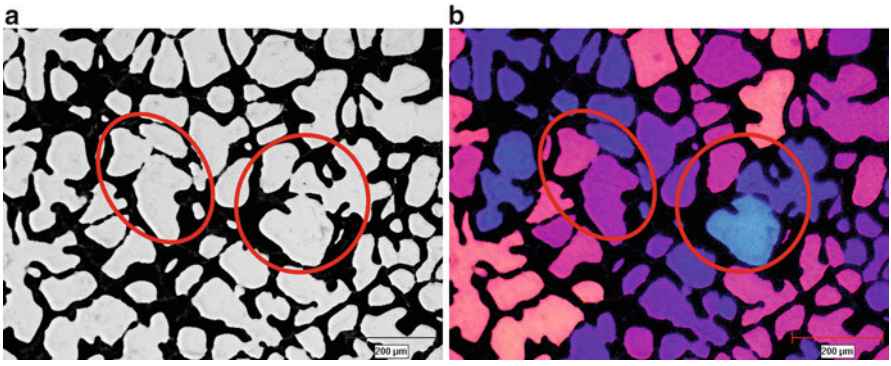

Fig. 4.40 Sintering effect of globules with bright field and with polarized light application, A356 alloy, quenched from 598 °C

small angle grain boundaries have lower energies and if formed with this condition, they could survive and remain in the microstructure.

An example of X-ray microtomography is shown in Fig. 4.41. Alloy Al–15.8% Cu was selected as solid and liquid phases in this alloy have good absorption contrast based on composition and the prepared specimen was held at 555 °C for 80 min while X-ray microtomography was carried out [116]. Two coarsening mechanisms were proposed. In one case, globules with very difference sizes were studied, Fig. 4.41a. The progressive dissolution of the small solid globule (1) is clearly seen (an Ostwald ripening like mechanism) however the coarsening of its neighbors is not large enough to be visible to the naked eye. The second coarsening mechanism is shown in Fig. 4.41b in case of equal size globules. While the neck size between particles 1 and 2 is increasing, necks between particles 2 and 3 or 2 and 4 remain stable. The neck diameter between particles 1 and 2 rapidly enlarges and the particles radii decrease slowly which is typical of coalescence and eventually leading into single particle [116].

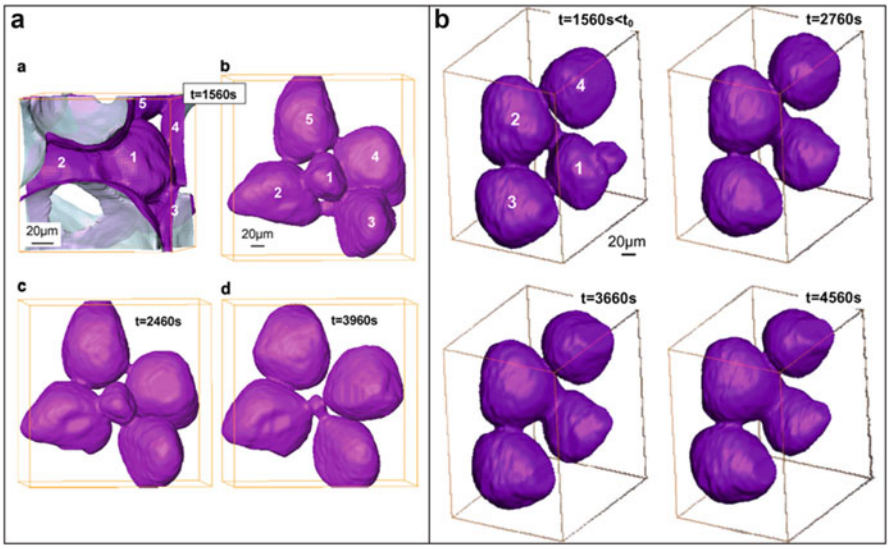

Fig. 4.41 X-ray microtomography of Al–15.8%Cu held at 555 °C for 80 min, (**a**) globules with various sizes, visible dissolution of globule 1 over time, (**b**) globule with equal size, coalescence toward formation of a single particle [116]

4.3.2 Quantitative Metallography

The application of polarized light microscopy provides a simple way to identify SSM structures as fully isolated globular or pseudo-globular morphologies including dendritic, degenerated dendritic, and rosette structures depending on the color contrast as mentioned and illustrated earlier. Once the distinction is made, image processing and analysis may be carried out to characterize the structure quantitatively [100].

Generally, it is assumed quantitative metallography is a simple technique; however, it should be remembered that there are a few but significant points where considering those should lead to acceptable results. According to the authors' experience, the major task during image analysis is the preparatory work done before processing and analyzing of the image. It means that by enhanced sample preparation including polishing and etching which is coupled with appropriate microscope selection and even working magnification, the resulting analyses would be reliable. For image analysis, the followings are of particular importance.

- Image acquisition
- Image enhancement
- Thresholding
- Image processing
- Data extraction

Thresholding is defined as the gray level of the image constituents. The better the difference in the gray levels, the more reliable results will be obtained. Therefore, the precision of the analysis depends on the thresholding limit and discriminating the unnecessary objects from the processed image. The main other issue is its repeatability which not only depends on the threshold setting, magnification, and light intensity and filtering but also on the sample preparation and using the same procedure in the metallographic preparation. Number of field of view (images) is another decisive parameter. By increasing the number of images captured and processed the errors become less and the results will be statistically reliable.

SSM processing is based on the formation of globules of the primary phase during solidification and as such the principal objectives are to quantify the volume fraction, size, and morphology of the primary particles. For morphology, the aspect ratio and sphericity number are proposed to be the most important factors to characterize particle shape while for size analysis average equivalent circular area diameter (the diameter of a circle having the same area as the particle being measured) is suggested.

4.3.2.1 Fraction Solid

Solid fraction is one of the main parameters in the rheological study and its variation alters the viscosity of the slurry. Solid fraction is measured in 2D polished surface (area fraction) and as mathematically shown (e.g., [117]), the volume fraction is equal to the mean value of area fraction. It is important to emphasize that the degree of the accuracy of the measurement is dependent on the number of field of view (images) analyzed.

Different methods are reported in the literature for measuring the fraction solid, among which the most commonly used ones are quantitative metallography, thermal analysis [118], lever rule (thermodynamic equilibrium condition), Scheil's equation [4], and application of software packages [119, 120]. The most common technique is quantitative metallography in which the sample that is rapidly quenched from SSM processing temperature to preserve the structure within the mushy zone is analyzed. The drawback is that the quenching is not rapid enough to prevent further growth of the solid particles and therefore the result is erroneous.

Thermal analysis is widely used to determine the solidification characteristics of metals and alloys. The technique could be divided into two groups: differential scanning calorimetry (DSC) and cooling curve analysis (CCA). Determination of latent heat is the typical application of DSC which is more accurate than the cooling curve analysis for many materials, including metals and alloys. DSC measures the energy (heat) evolved or absorbed by a sample as it is cooled, heated, or held at a temperature. However, DSC is limited to very small sample size, in the milligram range, and it is costly, requires technical expertise, and is not suitable for metallurgical or foundry shop floor operations. The alternative, cooling curve analysis (CCA), is simple, inexpensive, and most significantly suitable for commercial

applications. Briefly, the amount of heat evolved from a solidifying test sample is calculated by measuring the area between the first derivative curve and base line. This amount is proportional to the fraction solid [118]. This method is used in the Chap. 6 to identify the critical temperatures during the course of solidification.

Computational thermodynamic packages such as CALPHAD (CALculation of PHAse Diagram) are supplementary tools that provide quantitative data for multicomponent alloying systems. In this method, the Gibbs free energy of individual phases is modeled as a function of composition, temperature, critical magnetic temperature, and sometimes pressure and the results are gathered in a thermodynamic database. It enables the calculation of multicomponent phase diagrams and tracking of individual alloys during heat treatment process or solidification by calculation of phase distribution and composition [119, 120].

It is important to comprehend the shortcomings of each route when comparing the results calculated/measured by any of these techniques. The lever rule, Scheil, and thermal analysis routes may provide results different from that of quantitative microscopy. As for example in the case of Al7Si and A356 alloys (Al7Si0.35 Mg), quenching from 593 °C leads to higher solid fraction of about ~60 % (Fig. 4.42) which has almost a difference of 30 % from thermal analysis, Scheil, and lever rule [46, 121].

The large discrepancy may have its origin in the following sources:

- Inefficient quenching method. The formation of the eutectic colonies confirms the ineffectiveness of water quenching in stopping further transformation from liquid to solid. This could be initiated from the vapor layer usually forms around the billet to reduce heat extraction from the sample. It was tried to change the quenching media. Tzimas [44] have changed the quenching medium to liquid Sn–Pb eutectic, which is supposed to offer higher thermal diffusivity and good wettability, but the method was still unsuccessful and a greater solid fraction was observed after the quenching process. Furthermore, the residual liquid may also segregate on the prequenched primary solid particles during transferring the billet to the quenching station.
- Growth of the primary particles is another possibility for inaccuracy in the measurement. During transferring and quenching, the growth is constrained by the temperature profile in the liquid phase and this residual liquid may precipitate on the prequenched primary solid phase. Martinez and Flemings [122] stated that the additional spherical growth occurs during the quenching process is responsible for this overestimation. They have shown that a primary spherical globule in Al4.5%Cu with 40 μm diameter grows almost 40 μm in diameter during the quenching period.
- The effect of higher cooling rate which was missed in all the previous reports. With higher cooling rate, not only the liquids line shifts up (start of the primary dendrites nucleation temperature), but also the eutectic line shifts down and a larger solidification range results [46]. As seen in Fig. 4.43, by increasing the cooling rate, the primary α-Al phase increases. This would result in the formation of new primary particles and coarsening of the former primaries.

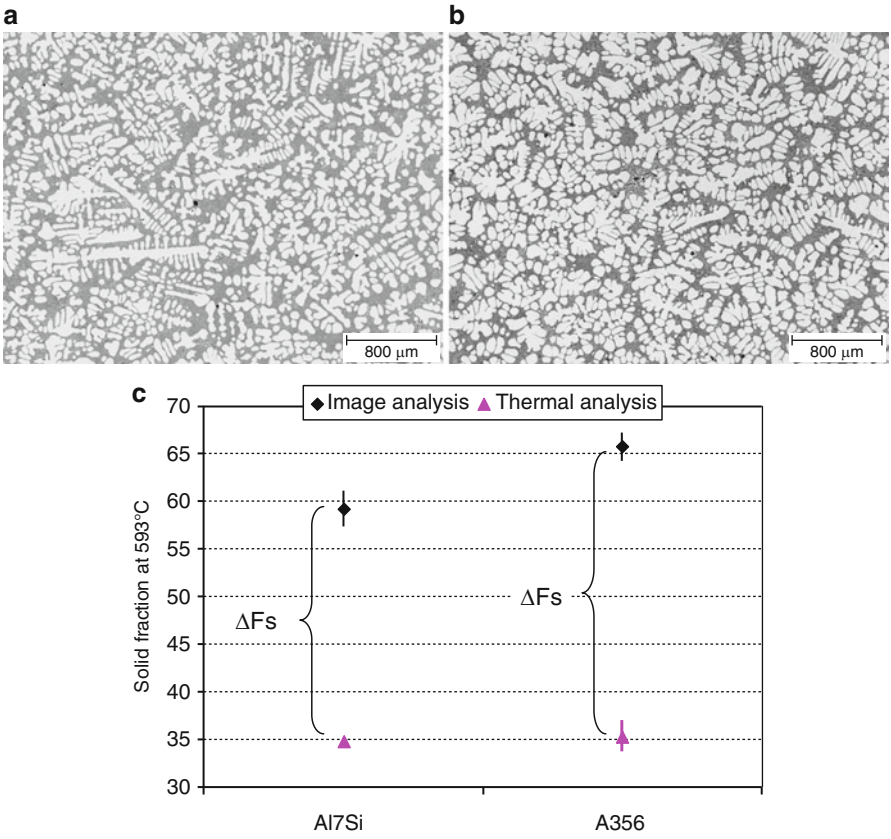

Fig. 4.42 Typical billet samples quenched from mushy zone at 593 ± 2 °C: (**a**) Al7Si, (**b**) A356, (**c**) solid fraction at ~593 °C, measured by thermal and image analyses [46] (ΔFs is the difference between two measurements)

4.3.2.2 Fraction of Entrapped Liquid

Liquid entrapment is a distinct feature of isothermal holding during semi-solid metal processing which normally is implemented during the thixocasting process. The first process occurring during isothermal holding of semi-solid structure is grain coarsening. In dendritic structure, the dendritic arms disappear by ripening and coalescence which has been already discussed in Chap. 3. The coalescence of isolated globules from same dendrite (same crystallographic orientation) or coalescence of neighboring arms may result in liquid metal entrapment (Fig. 4.44). The "entrapped liquid" adversely affects the deformability of material which is associated to a reduction in the interconnected liquid phase and therefore influences the rheological behavior of the slurry.

Volume of entrapped liquid depends on various parameters including semi-solid processing, cooling rate and morphology of as-cast structure, reheating time, and

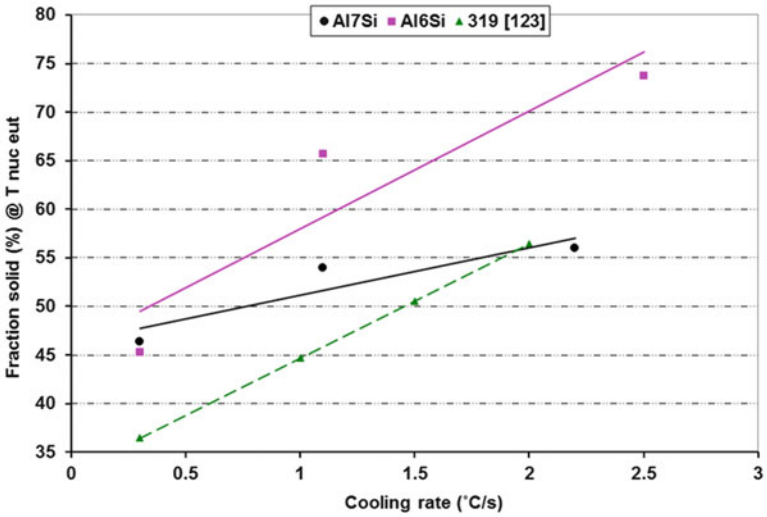

Fig. 4.43 Effect of various cooling rate on fraction solid, Al7%Si, Al6%Si, and 319 alloy (319 alloy data from [123])

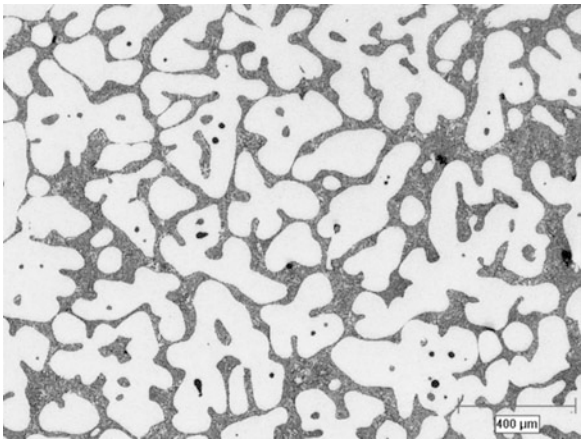

Fig. 4.44 Optical micrograph showing entrapped liquids, A356 cast in graphite mold, reheated and isothermally held for 10 min @583 °C

temperature. In fact contrary to its name, sometimes these pools which seem to be encapsulated in 2D surface may be interconnected in the volume.

4.3.2.3 Particle Size, Average Circular Diameter

The ideal microstructure for SSM processing is the one free from dendrites and having homogenous spherical particles. The globule size plays an important role on the castability and mechanical properties of the as-cast parts. However, it is important to factor in that the primary solid is a softer phase and minimizing its

size is crucial for achieving the desired mechanical properties. As a general guideline, the optimum primary particle size reported for SSM alloys is less than 100 μm [124].

It is worth noting that image analysis technique has limited capabilities. Therefore, it should always be kept in mind that what image analysis cannot do, for instance, the definition of diameter in the software is based on the equation ($d = 2\sqrt{A/\pi}$), which A refers to the area of the object(s) being measured. Such measurement makes the assumption that the examined object has a shape close to a circle and for instance, the more the particle is rectangular, the greater is the error in the calculation (in this case, aspect ratio is a better parameter). Considering this point, it should be expected to detect small difference between the average circular diameter of a rosette and globule α-Al particle with the same area.

As indicated earlier in this chapter and with highlighting the disability of image analysis, it should always keep in mind that the analysis system could not distinguish between dendrite branches and individual globules. Therefore in case of dendritic structure, calculation will result in a lower value for circular diameter or rise in sphericity number which is an error source. In some cases, grain and globule sizes should be measured individually.

Technically, there are two different definitions for globule and grain size. Globules are primary particles which are apparently detached from one another. However, by applying polarized light microscopy, it becomes clear that the neighboring individual particles might be interconnected from underneath of the polished surface (having the same crystallographic orientation relationship). As a result, similar color neighboring globules specify a particular grain. By this method, grains could be differentiated from globules. Figure 4.45 shows an EMS stirred sample which is isothermally held at 583 °C for 10 min. Selected grains and globules are clearly shown.

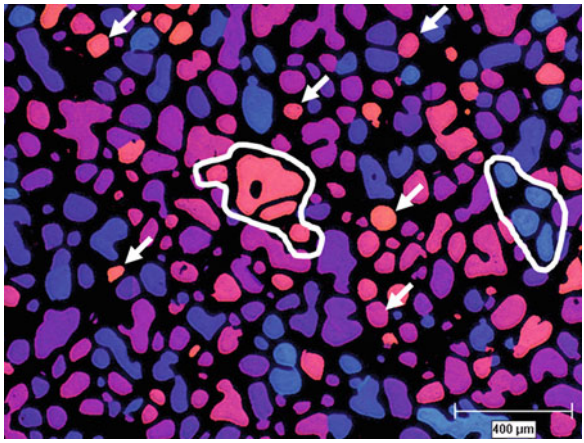

Fig. 4.45 EM stirred Al7Si0.8Fe isothermally held at 593 °C, Copper mold cast at 630 °C (*arrowed*: globules, *circled*: grains)

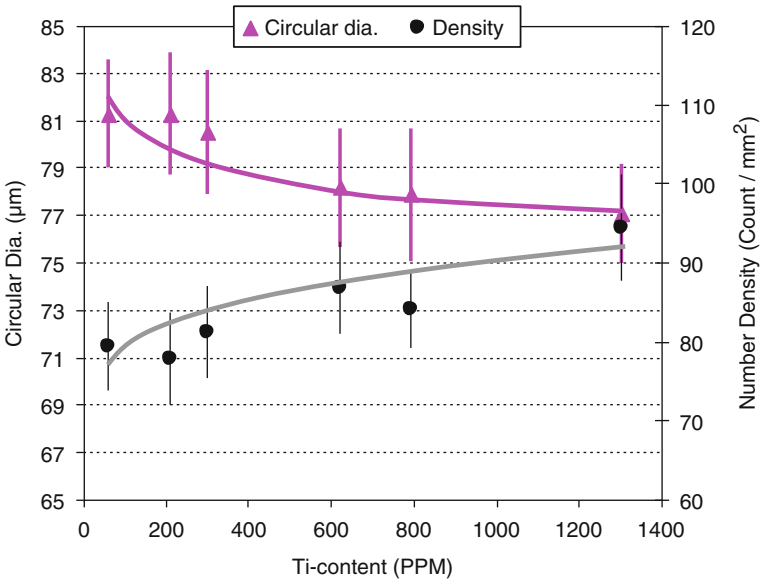

Fig. 4.46 Average circular diameter and number density for A356 with Ti and B addition (reproduced from [125])

4.3.2.4 Number Density

In some cases, it is necessary to have an estimation of the quantity of particles within a unit area, number density (mm^{-2}). Higher value of number density specifies smaller particles within the area. For instance, addition of grain refiner results in more effective nucleation sites which leads to limited growth and better distribution of primary particles. This is presented in Fig. 4.46 where with addition of AlTiB master alloy to A356 alloy, the density of primary particles increased. Figure 4.46 also shows number density increases when there are particles with smaller circular diameter [125].

4.3.2.5 Sphericity/Shape Factor

Primary particles' shape is a key factor in quantitative metallography affecting the viscosity of semi-solid slurry. Physically rounder particles have better flowability in comparison to rectangular ones. Sphericity is given by $\frac{4\pi A}{P^2}$ where A is the total area of primary particles and P represents perimeter of liquid–primary particles interface. The sphericity factor varies between 0 for objects having very elongated cross sections and 1 for those having circular cross sections. By using the average value of sphericity, it was concluded that this parameter is not responsive to small variation of the morphology and in most cases due to the averaging of numerous particle sphericity; the maximum difference is less than 0.1. Therefore, a more sensitive parameter was chosen which is the percentage of particles having sphericity greater than a certain value.

4.3.2.6 Specific Volume Surface

Also known as surface area per unit volume, it can be used to define the success of SSM process in producing individual particle which means having larger S_v. S_v is mathematically expressed as $S_v = \frac{4}{\pi}\frac{P}{A}$ where A is the total area of primary particles and P represents perimeter of liquid–primary particles interface. $\frac{A}{P}$ is a parameter which could be used for quantitative metallography which is inversely proportional to S_v.

4.3.2.7 Aspect Ratio

Aspect ratio is simply defined as the ratio of the longest over the shortest feret diameters, length per width. Feret diameter is defined as the distance between two parallel tangents on each side of an object (Fig. 4.47a). Values near one (1) are characteristics of spherical particles while higher values show more elongated (needle) like particles. Figure 4.47b provides aspect ratios of 356 Al–Si alloy slurry prepared at various pouring temperatures. For overstressing the effect of pouring temperature, the percentage of particles having aspect ratio greater than 2 is presented. With increasing the pouring temperature, the formation of elongated particles is promoted which is an indication of dendritic structure.

4.3.3 Microscopy/Image Analysis Setup

For characterizing the α-Al particles, 85 fields with the total area of 255 mm^2 were examined (Mag. ×50); while for evaluating of silicon morphology in graphite cups, 50 fields with 1.48 mm^2 were scanned (Mag. ×500). In the EMS samples and by

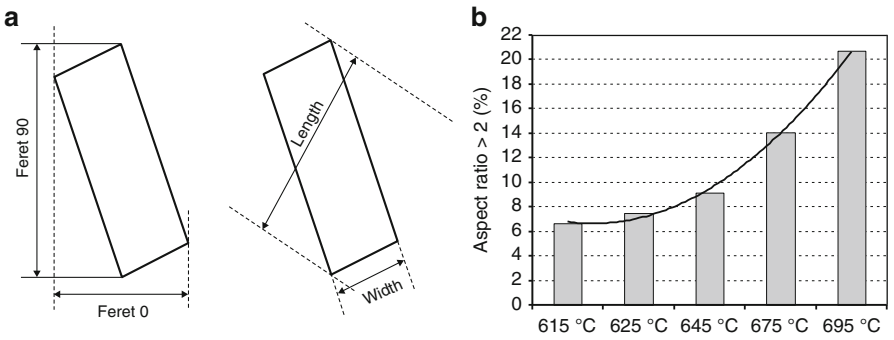

Fig. 4.47 (**a**) Definitions of feret, length, and width [100], (**b**) percentage of particles having aspect ratio greater than 2 [67]

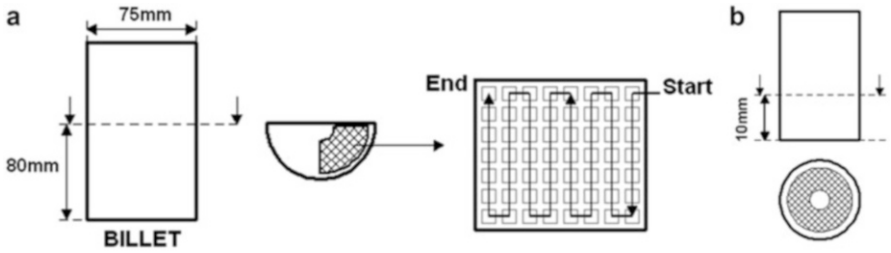

Fig. 4.48 (**a**) Area for quantitative analysis for SSM billets and applied scanning mode, (**b**) Area for quantitative analysis for conventional casting, graphite cup

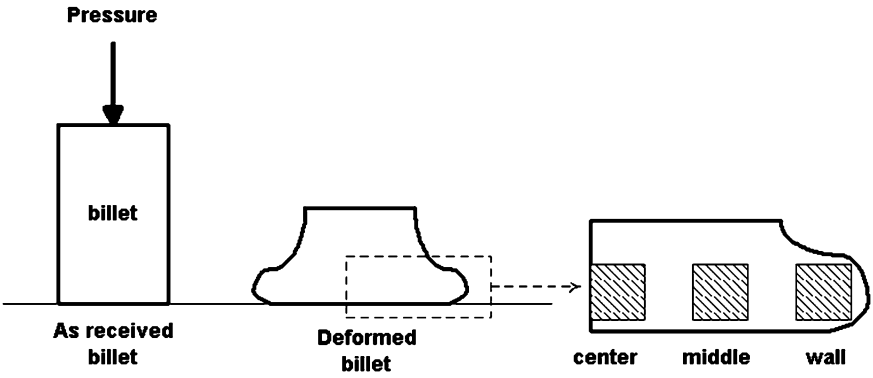

Fig. 4.49 Area for optical micrographs observations for a typical deformation

considering using different cooling rates, it was impossible to work at the same magnification and thus for sand and copper castings 50 and 80 fields at ~×200 and ~×500 magnifications with a total area of 9.3 and 2.3 mm^2 were used respectively. In aluminum alloys, the best resolution of individual grains could be achieved by examining electrolytically anodized specimens by polarized light microscopy. For grain size measurement, samples were polarized by fluoboric acid solution[5] and measurements were done between the wall and center of the graphite cup sample, Fig. 4.48.

In the case of rheological tests, the microstructure was studied on the longitudinal sections within the regions with the highest deformation rate as shown schematically in Fig. 4.49.

[5]In this method, a film of Al2O3 is deposited on the surface which its thickness depends mainly on the crystallographic orientation of the grain(s). When the sample is viewed by a polarized light which is passing through the analyzer, the film can rotate the plane of polarization regarding the orientation of the underlying grain and consequently producing various shades of colors by inserting a sensitive tint plate [113].

References

1. L. Backerud, G. Chai, J. Tamminen, *Solidification Characteristics of Aluminum Alloys, Volume 2, Foundry Alloys* (American Foundry Society, Des Plaines, 1990)
2. B.L. Tuttle, AFS Thermal Analysis Committee, Definitions in thermal analysis. Modern Casting (Nov 1985), 39–41
3. D. Gloria, Control of grain refinement of Al-Si alloys by thermal analysis. PhD Thesis, Department of Mining and Metallurgical Engineering, McGill University, Canada, June 1999
4. M.C. Flemings, *Solidification Processing* (McGraw-Hill, New York, 1974)
5. B.J. Yang, D. Stefanescu, J. Leon-Torres, Modeling of microstructural evolution with tracking of equiaxed grain movement for multicomponent Al-Si Alloy. Metal. Trans. A **32**, 3065–3076 (2001)
6. Norax, Canada http://www.noraxcanada.com
7. D.B. Spencer, R. Mehrabian, M.C. Flemings, Rheological behavior of Sn-15 Pct Pb in the crystallization range. Metal. Trans. **3**, 1925–1932 (1972)
8. R. Mehrabian, M.C. Flemings, Die castings of partially solidified alloys. AFS Trans. **80**, 173–182 (1972)
9. J.R. Van Wazer, R.E. Colwell, *Viscosity and Flow Measurement* (Wiley Interscience, New York, 1966)
10. D.R. Poirier, G.H. Geiger, *Transport Phenomena in Materials Processing* (TMS, Warrendale, 1994)
11. J.W. Goodwin, R.W. Hughes, *Rheology for Chemists, An Introduction* (Royal Society of Chemistry, London, 2000)
12. J.D. Ferry, *Viscoelastic Properties of Polymers* (Wiley, New York, 1970)
13. J. Campbell, *Casting* (Butterworth-Heinemann, Oxford, 1991). Chap. 2
14. Y.D. Kwon, Z.H. Lee, The effect of grain refining and oxide inclusion on the fluidity of Al-4.5Cu-0.6 Mn and A356 alloys. Mater. Sci. Eng. **A360**, 372–376 (2003)
15. A. Assar, N. El-Mahllawy, M.A. Taha, Fluidity of stir-cast Al-10% Cu alloy. Aluminum **57**, 807–810 (1981)
16. M. Suéry, *Mise en Forme des alliages métalliques a l'état semi solide* (Lavoisier, France, 2002)
17. M.C. Flemings, Behavior of metal alloys in the semi-solid state. Metal. Trans. A **22A**, 952–981 (1991)
18. D.H. Kirkwood, Semisolid metal processing. Int. Mater. Rev. **39**, 173–189 (1994)
19. Z. Fan, Semisolid metal processing. Int. Mater. Rev. **47**(2), 49–85 (2002)
20. H.V. Atkinson, Modelling the semisolid processing of metallic alloys. Progr. Mater. Sci. **50**, 341–412 (2005)
21. M.J. Stefan, Versuche Uber Die Scheinbare Adhasion SitzberMth. Naturw. Kl. Bagar Akad. Wiss Munchen **69**, Part 2 (1874)
22. X. Yang, Y. Jing, J. Liu, The rheological behavior for thixocasting of semi-solid aluminum alloy (A356). J. Mater. Proc. Tech. **130–131**, 569–573 (2002)
23. W. Nan, S. Guangji, Y. Hanguo, Rheological study of partially solidified Tin-Lead and Aluminum-Zinc alloys for stir casting. Mater. Trans. JIM **31**(8), 715–722 (1990)
24. R. Ghomashchi, *An Introduction to Engineering Materials* (University of South Australia, Australia, 1999)
25. R. Zehe, First production machine for rheocasting. Light Met. Age **57**(9), 62–66 (1999)
26. A. Beaulieu, L. Azzi, F. Ajersch, S. Turenne, F. Pineau, C.A. Loong, Numerical modeling and experimental analysis of die cast semi-solid A356 alloy, in *Proceeding of M.C. Flemings on Solidification and Materials Processing*, ed. by R. Abbaschian, H. Brody, A. Mortensen (TMS, Warrendale, 2001), 261–265
27. A. Wahlen, Modelling the processing of aluminum alloys in the semi-solid state. Mater. Sci. Forum **396–402**, 185–190 (2002)

28. M. Modigell, J. Koke, Rheological modelling on semi-solid metal alloys and simulation of thixocasting processes. J. Mater. Proc. Tech. **111**, 53–58 (2001)
29. C.G. Kang, H.K. Jung, A study on thixoforming process using the thixotropic behavior of an aluminum alloy with an equiaxed microstructure. J. Mater. Eng. Perform. **9**(5), 530–535 (2000)
30. M.C. Flemings, R.G. Riek, K.P. Young, Rheocasting processes. AFS Int. Cast Metals J. **1**(3), 11–22 (1976)
31. K. Brissing, K. Young, Semi-solid casting machines, heating systems, properties and applications. Die Casting Eng. **44**(6), 34–41 (2000)
32. T.Z. Kattamis, T.J. Piccone, Rheology of semi solid Al-4.5%Cu-1.5%Mg alloy. Mater. Sci. Eng. **A131**, 265–272 (1991)
33. D. Brabazon, D.J. Browne, A.J. Carr, Experimental investigation of the transient and steady state rheological behavior of Al-Si alloys in the mushy state. Mater. Sci. Eng. **A356**, 69–80 (2003)
34. J.Y. Chen, Z. Fan, Modeling of rheological behavior of semisolid metal slurries, part 1—theory. Mater. Sci. Technol. **18**, 237–242 (2002)
35. P.A. Joly, R. Mehrabian, The rheology of partial solid alloys. J. Mater. Sci. **11**, 1393–1403 (1976)
36. O. Lashkari, R. Ghomashchi, F. Ajersch, Deformation behavior of semi-solid A356 Al-Si alloy at low shear rates: the effect of sample size. Mater. Sci. Eng. **A444**, 198–205 (2007)
37. O. Lashkari, R. Ghomashchi, Deformation behavior of semi-solid A356 Al-Si alloy at low shear rates: effect of morphology. Mater. Sci. Eng. **A454–455**, 30–36 (2007)
38. O. Lashkari, R. Ghomashchi, Deformation behavior of semi-solid A356 Al-Si alloy at low shear rates: effect of fraction solid. Mater. Sci. Eng. **A486**, 333–340 (2008)
39. C.L. Martin, P. Kumar, S. Brown, Constitutive modeling and characterization of the flow behavior of semi-solid metal alloy slurries-II. Structural evolution under shear formation. Acta Metall. Mater. **42**(11), 3603–3614 (1994)
40. O. Lashkari, R. Ghomashchi, The implication of rheology in semi-solid metal processes: an overview. J. Mater. Proc. Tech. **182**, 229–240 (2007)
41. O. Lashkari, R. Ghomashchi, Evolution of primary α-Al particles during isothermal transformation of rheocast semi solid metal billets of A356 Al-Si alloy. Canad. Metall. Quart. **53**, 47–54 (2014)
42. H.V. Atkinson, D. Liu, Coarsening rate of microstructure in semi-solid aluminium alloys. Trans. Nonferrous Met. Soc. China **20**, 1672–1676 (2010)
43. M. Perez, J.C. Barbe, Z. Neda, Y. Brechet, L. Salvo, M. Suery, Investigation of the microstructure and the rheology of semi-solid alloys by computer simulation. J. Phys. IV France **11**, 93–100 (2001)
44. E. Tzimas, A. Zavaliangos, Evaluation of volume fraction of solid in alloys formed by semisolid processing. J. Mater. Sci. **35**, 5319–5329 (2000)
45. Y. Zhu, J. Tang, Y. Xiong, Z. Wu, C. Wang, D. Zeng, The influence of the microstructure morphology of A356 alloy on its rheological behavior in the semisolid state. Sci. Tech. Adv. Mater. **2**, 219–223 (2001)
46. S. Nafisi, D. Emadi, R. Ghomashchi, Semi solid metal processing: the fraction solid dilemma. Mater. Sci. Eng. **A507**(1–2), 87–92 (2009)
47. J.Y. Chen, Z. Fan, Modeling of rheological behavior of semisolid metal slurries, part 3—transient state behavior. Mater. Sci. Technol. **18**, 250–257 (2002)
48. G. Chai, T. Roland, L. Arnberg, L. Backerud, Studies of dendrite coherency in solidifying aluminum alloy melts by rheological measurements. in *Second International Conference, Semi-Solid Processing of Alloys and Composites* (Cambridge, 1992), 193–201
49. O. Lashkari, R. Ghomashchi, The implication of rheological principles for characterization of semi-solid Al-Si cast billets. J. Mater. Sci. **41**, 5958–5965 (2006)
50. Z. Fan, J.Y. Chen, Modelling of rheological behavior of semisolid metal slurries, part 4—effects of particle morphology. Mater. Sci. Technol. **18**, 258–267 (2002)

51. S. Jabrane, B. Clement, S. Ajersch, Evolution of primary particle morphology during rheoprocessing of Al-5.2%Si alloy. in *Second International Conference, Semi-Solid Processing of Alloys and Composites* (Cambridge, 1992), 223–236
52. M. Silva, A. Lemieux, H. Blanchette, X. Chen, The determination of semi-solid processing ability using a novel rheo-characterizer apparatus. In *10th International Conference on Semi-Solid Processing of Alloys and Composites* (Aachen, Germany, 2008) (published in Solid State Phenomena, vol. 141–143, 2008, 343–348)
53. E.J. Zoqui, M. Paes, M.H. Robert, Effect of macrostructure and microstructure on the viscosity of the A356 alloy in the semi-solid state. J. Mater. Proc. Tech. **153–154**, 300–306 (2004)
54. M. Mada, F. Ajersch, Rheological model of semisolid A356-SiC composite alloys. Part I. Dissociation of agglomerate structures during shear. Mater. Sci. Eng. A **212**, 157–170 (1996)
55. M. Mada, F. Ajersch, Rheological model of semisolid A356-SiC composite alloys. Part II. Reconstitution of agglomerate structures at rest. Mater. Sci. Eng. A **212**, 171–177 (1996)
56. T.Y. Liu, P.J. Ward, D.H. Kirkwood, H.V. Atkinson, Rapid compression of aluminium alloys and its relationship to thixoformability. Int. Mater. Rev. **34**, 409–417 (2003)
57. M. Modigell, L. Pape, M. Hufschmidt, Kinematics of structural changes in semisolid alloys by shear and oscillation experiments. in *8th International Conference on Semi-Solid Processing of Alloys and Composites* (Limassol, Cyprus, 2004)
58. S. Sannes, L. Arnberg, M.C. Flemings, Orientational relationships in semi-solid Al-6.5wt% Si, in *Light Metals*, ed. by W. Hale (TMS, Anaheim, 1996), 795–798
59. Z. Fan, J.Y. Chen, Modeling of rheological behavior of semisolid metal slurries, part 2—steady state behavior. Mater. Sci. Technol. **18**, 243–249 (2002)
60. L. Arnberg, A. Bardal, H. Sund, Agglomeration in two semisolid type 6082 aluminum alloys. Mater. Sci. Eng. **A262**, 300–303 (1999)
61. M. Hirai, K. Takebayashi, Y. Yoshikawa, Effect of chemical composition on apparent viscosity of Semi-solid alloys. ISIJ Int. **33**(11), 1182–1189 (1993)
62. M. Hirai, K. Takebayashi, Y. Yoshikawa, R. Yamaguchi, Apparent viscosity of Al-10mass% Cu semi-solid alloys. ISIJ Int. **33**(3), 405–412 (1993)
63. H. Wang, C.J. Davidson, J.A. Taylor, D.H. St John, Semisolid casting of AlSi7Mg0.35 alloy produced by low temperature pouring. Mater. Sci. Forum **396–402**, 143–148 (2002)
64. W. Mao, C. Cui, A. Zhao, J. Yang, X. Zhong, Effect of pouring process on the microstructure of semi solid AlSi7Mg alloy. Mater. Sci. Eng. **17**(6), 615–619 (2001)
65. K. Xia, G. Tausig, Liquidus casting of a wrought aluminum alloy 2618 for thixoforming. Mater. Sci. Eng. **A246**, 1–10 (1998)
66. S. Midson, K. Young, Impact of casting temperature on the quality of components semi-solid metal cast form alloys 319 and 356. in *5th AFS International Conference of Molten Aluminum* (1998), 409–422
67. O. Lashkari, S. Nafisi, R. Ghomashchi, Microstructural characterization of rheo-cast billets prepared by variant pouring temperatures. Mater. Sci. Eng. **A441**, 49–59 (2006)
68. D. Doutre, G. Hay, P. Wales, J.P. Gabathuler, SEED: a new process for semi solid forming. in *Light Metals Conference, COM 2003*, ed. by J. Masounave, G. Dufour (Vancouver, Canada), 293–306
69. D. Bouchard, F. Pineau, D. Doutre, P. Wales, J. Langlais, Heat transfer analysis of swirled enthalpy equilibration device for the production of semi-solid aluminum. in *Light Metals Conference, COM 2003*, ed. by J. Masounave, G. Dufour (Vancouver, Canada), 229–241
70. H.I. Lee, R.D. Doherty, E.A. Feest, J.M. Titchmarsh, Structure and segregation of stir-cast aluminum alloys, The Metals Society. in *Proceeding of International Conference, Solidification Technology in Foundry and Cast House* (UK, 1983), 119–125
71. D. Brabazon, D.J. Browne, A.J. Carr, J.C. Healy, Design, construction, and operation of a combined rheocaster/rheometer. in *Fifth International Conference on Semi-Solid Processing of Alloys and Composites* (Golden, 1998), 21–28

72. O. Lashkari, R. Ghomashchi, F. Ajersch, Rheological study of 356 Al-Si foundry alloy prepared by a new innovative SSM process. in *EPD Congress*, ed. by Mark E. Schlesinger (TMS, Warrendale, 2005), 149–156
73. P.R. Prasad, A. Prasad, C.B. Singh, Calculation of primary particle size in rheocast slurry. J. Mater Sci. Lett. **14**, 861–863 (1995)
74. E.A. Vieira, A.M. Kliauga, M. Ferrante, Microstructural evolution and rheological behavior of aluminum alloys A356, and A356 + 0.5% Sn designed for thixocasting. J. Mater. Proc. Tech. **155–156**, 1623–1628 (2004)
75. V. Laxmanan, M.C. Flemings, Deformation of semi-solid Sn-15 Pct Pb alloy. Metal. Trans. A **11A**, 1927–1937 (1980)
76. L. Azzi, F. Ajersch, Development of aluminum-base alloys for forming in semi solid state. in *TransAl Conference* (Lyon, France, 2002), 23–33
77. H. Mirzadeh, B. Niroumand, Fluidity of Al-Si semisolid slurries during rheocasting by a novel process. J. Mater. Proc. Tech. **209**, 4977–4982 (2009)
78. S. Nafisi, O. Lashkari, R. Ghomashchi, A. Charette, Effect of different fraction solids on the fluidity of rheocast 356 Al-Si alloy. in *Multi Phase Phenomena and CFD Modeling and Solidification in Materials Processes* (TMS, North Carolina, 2004), 119–128
79. Y. Murakami, K. Miwa, M. Kito, T. Honda, N. Kanetake, S. Tada, Effects of injection conditions in the semi-solid injection process on the fluidity of JIS AC4CH aluminum alloy. Mater. Trans. **54**(9), 1788–1794 (2013)
80. J. Wannasin, D. Schwam, J.A. Yurko, C. Rohloff, G. Woycik, Hot tearing susceptibility and fluidity of semi solid gravity cast Al Cu alloy. in *Ninth International Conference on Semi-Solid Processing of Alloys and Composites* (Busan, Korea, 2006) (published in Solid State Phenomena, vol. 116–117, 2006, 76–79)
81. M. Forte, D. Bouchard, A. Charette, Fluid flow investigation of die cast tensile test bars. in *Ninth International Conference on Semi-Solid Processing of Alloys and Composites* (Busan, Korea, 2006) (published in Solid State Phenomena, vol. 116–117, 2006, 457–463)
82. T. Haga, H. Fuse, Semi-solid die casting of Al-25%Si. in *13th International Conference on Semi-Solid Processing of Alloys and Composites* (Muscat, Oman, 2014) (published in Solid State Phenomena, vol. 217–218, 2015, 436–441)
83. F. Kolenda, P. Retana, G. Racineux, A. Poitou, Identification of rheological parameters by the squeezing test. Powder Tech. **130**, 56–62 (2003)
84. J.A. Yurko, M.C. Flemings, Rheology and microstructure of semi-solid aluminum alloys compressed in the drop forge viscometer. Metal. Trans. A **33A**, 2737–2746 (2002)
85. M. Suéry, M.C. Flemings, Effect of strain rate on deformation behavior of semi-solid dendritic alloys. Metal. Trans. A **13A**, 1809–1819 (1982)
86. Y. Fukui, D. Nara, N. Kumazawa, Evaluation of the deformation behavior of a semi-solid hypereutectic Al-Si alloy compressed in a drop-forge viscometer. Metal. Trans. A **46A**, 1908–1916 (2015)
87. J.H. Han, D. Feng, C.C. Feng, C.D. Han, Effect of sample preparation and flow geometry on the rheological behavior and morphology of micro phase-separated block copolymers: comparison of cone-and-plate and capillary data. Polymer **36**, 155–167 (1995)
88. W.M. Gearhart, W.D. Kennedy, Cellulose acetate butyrate plastics. Indus. Eng. Chem. **41**(4), 695–701 (1949)
89. G.H. Dienes, H.F. Klemm, Theory and application of the parallel plate plastometer. J. Appl. Phys. **17**, 458–464 (1946)
90. O. Draper, S. Blackburn, G. Dolman, K. Smalley, A. Griffiths, A comparison of paste rheology and extrudate strength with respect to binder formulation and forming technique. J. Mater. Proc. Tech. **92–93**, 141–146 (1999)
91. S. Turenne, N. Legros, S. Laplante, F. Ajersch, Mechanical behavior of Aluminum matrix composite during extrusion in the semisolid state. Metal. Trans. A **30A**, 1137–1146 (1999)
92. M. Ferrante, E. de Freitas, Rheology and microstructural development of Al-4wt%Cu alloy in the semi solid state. Mater. Sci. Eng. **A271**, 172–180 (1999)

93. M. Ferrante, E. de Freitas, M. Bonilha, V. Sinka, Rheological properties and microstructural evolution of semi-solid aluminum alloys inoculated with Mischmetal and with Titanium. in *Fifth International Conference on Semisolid Processing of Alloys and Composites* (1998), 35–42
94. H. Blanchette, Development a quality control method for Aluminum semi solid billet obtained from the SEED process. M. Eng Thesis, University of Quebec, Canada, 2006
95. O. Lashkari, R. Ghomashchi, A new machine to characterize microstructural evolution of semi solid metal Billets through viscometry. Mater. Design **28**(4), 1321–1325 (2007)
96. J.D. Sherwood, Squeeze flow of a Herschel-Bulkley fluid. J. Newtonian Fluid Mech. **77**, 115–121 (1998)
97. J.D. Sherwood, D. Durban, Squeeze flow of a power-law viscoplastic solid. J. Non-newtonian Fluid Mech. **62**, 35–54 (1996)
98. J.P. Gabathuler, Evaluation of various processes for the production of billets with thixotropic properties. in *Proceeding of 2nd Conference of Semi solid Materials* (1992), 33–46
99. D.J. Lahaie, M. Bouchard, Physical modeling of the deformation mechanisms of semisolid bodies and a mechanical criterion for hot tearing. Metal. Trans. B **32B**, 697–705 (2001)
100. S. Nafisi, R. Ghomashchi, The microstructural characterization of semi-solid slurries. JOM **58**(6), 24–30 (2006)
101. Oxford instruments www.ebsd.com
102. OIM Analysis Tutorials, Ametek, Inc.
103. B. Niroumand, K. Xia, 3D study of the structure of primary crystals in a rheocast Al-Cu alloy. Mater. Sci. Eng. A **283**, 70–75 (2000)
104. J. Alkemper, P.W. Voorhees, Three-dimensional characterization of dendritic microstructures. Acta. Mater. **49**, 897–902 (2001)
105. T.L. Wolfsdorf, W.H. Bender, P.W. Voorhees, The morphology of high volume fraction solid-liquid mixtures: an application of microstructural tomography. Acta. Mater. **45**(6), 2279–2295 (1997)
106. Y. Ito, M.C. Flemings, J.A. Cornie, Rheological behavior and microstructure of Al-6.5wt%Si alloy. in *Nature and Properties of Semi-Solid Materials*, ed. by J.A. Sekhar, J. Dantzig (TMS, Warrendale, 1991), 3–17
107. Private communication with Prof. Xiangjie Yang, School of Mechanical Engineering, Nanchang University, China, 2016
108. L. Salvo, M. Suery, A. Marmottant, N. Limodin, D. Bernard, 3D imaging in material science: application of X-ray tomography. Comptes Rendus Phys. **11**, 641–649 (2010)
109. K.M. Kareh, In situ synchrotron tomography of granular deformation in semi solid Al Cu alloys. PhD Thesis, Imperial College London, Sep 2013
110. G.C. Gu, R. Pesci, L. Langlois, E. Becker, R. Bigot, M.X. Guo, Microstructure observation and quantification of the liquid fraction of M2 steel grade in the semi solid state, combining confocal laser scanning microscopy and X-ray microtomography. Acta Mater. **66**, 118–131 (2014)
111. W. Xu, M. Ferry, N. Mateescu, J.M. Cairney, F.J. Humphreys, Techniques for generating 3-D EBSD microstructures by FIB tomography. Mater. Character. **58**, 961–967 (2007)
112. Z. Zaafarani, D. Raabe, R.N. Singh, F. Roters, S. Zaefferer, Three dimensional investigation of the texture and microstructure below a nanoindent in a Cu single crystal using 3D EBSD and crystal plasticity finite element simulations. Acta Mater. **54**, 1863–1876 (2006)
113. G. Vander Voort, *Metallography, Principles and Practice* (ASM International, Materials Park, 1999)
114. A. Apaydin, K.V. Prabhakar, R.D. Doherty, Special grain boundaries in Rheocast Al-Mg. Mater. Sci. Eng. **46**, 145–150 (1980)
115. R.D. Doherty, H.I. Lee, E.A. Feest, Microstructure of stir-cast metals. Mater. Sci. Eng. **A65**, 181–189 (1984)

116. N. Limodin, L. Salvo, M. Suery, M. DiMichiel, In situ investigation by X-ray Tomography of the overall and local microstrucutral changes occurring during partial remelting of an Al158 wt Cu alloy. Acta Mater. **57**, 2300–2310 (2009)
117. R.T. DeHoff, F.N. Rhines, *Quantitative Microscopy* (McGraw-Hill, New York, 1968)
118. D. Emadi, L.V. Whiting, S. Nafisi, R. Ghomashchi, Applications of thermal analysis in quality control of solidification processes. J. Thermal Anal. Calorimetry **81**, 235–242 (2005)
119. N. Saunders, A.P. Miodownik, *CALPHAD (Calculation of Phase Diagram): A Comprehensive Guide* (Elsevier, Oxford, 1998)
120. B. Sundman, *ThermoCalc Version L User's Guide, Division of Computational Thermodynamic* (Department of Material Science and Engineering, Royal Institute of Technology, Stockholm, 1996)
121. S. Nafisi, R. Ghomashchi, A. Charette, Effects of grain refining on morphological evolution of Al-7%Si in the swirled enthalpy equilibration device (SEED). in *66th World Foundry Congress* (Turkey, Sep 2004), 1253–1263
122. R.A. Martinez, M.C. Flemings, Evolution of particle morphology in semisolid processing. Metal. Trans. A **36A**, 2205–2210 (2005)
123. R.I. MacKay, M.B. Djurdjevic, J.H. Sokolowski, Effect of cooling rate on fraction solid of metallurgical reactions in 319 alloy. AFS Trans. **108**, 521–530 (2000)
124. D. Apelian, Semi-solid processing routes and microstructure evolution. in *7th International Conference on Semi-Solid Processing of Alloys and Composites* (Tsukuba, Japan, 2002), 25–30
125. S. Nafisi, R. Ghomashchi, Grain refining of conventional and semi-solid A356 Al-Si alloy. J. Mater. Proc. Tech. **174**, 371–383 (2006)